The role of the dynamic pressure in the behavior of an oscillating gas bubble

The role of the dynamic pressure in the behaviour of an oscillating gas bubble

F. Brini* and L. Seccia*
Department of Mathematics, University of Bologna via Saragozza,8 I-40123 Bologna Italy
(*Author to whom the correspondence should be addressed: francesca.brini@unibo.it.)
(Dated: October 25, 2024)

The paper contains a preliminary study on the role that dynamic pressure might play in the dynamics of a gas bubble oscillating in a liquid. To this aim we introduce a mathematical model, proposed under the homobaricity hypothesis and deduced from the 14-moment theory of rational extended thermodynamics through significant simplifications, that makes the equations easily integrable over long time intervals. In the presence of a gas with high bulk viscosity, relevant effects can be observed in different physical conditions: isothermal or adiabatic regimes, small amplitude oscillations, non-linear oscillations, resonances and sonoluminescence. To make the study more realistic, we always refer to carbon dioxide gas, which on the one hand could present high values of bulk viscosity and on the other hand is known for its peculiar behaviours in the framework of cavitation and gas bubbles.

I. INTRODUCTION

For more than a century, the phenomena associated with gas bubbles in a liquid have fascinated researchers from several fields, so much so that an enormous amount of literature is available on the various aspects associated with cavitation, non-linear oscillations of such bubbles in the presence of an acoustic pressure, sonoluminescence (i.e. the appearance of a light flash during the oscillations of one or more bubbles under suitable physical conditions)[1–10]. If the studies initially concerned natural effects and phenomena linked to cavitation – think for example of Lord Rayleigh's initial work on the damage caused by cavitation on ship propellers [1]– recently the focus was shifted to applications in medicine, sonochemistry and engineering, exploiting the bizarre behaviours of gas bubbles (sometimes tiny in size and other times very large). Unfortunately, it is impossible here to offer a complete picture of the literature or at least to enumerate the very notable applications in the medical field that are under study and seem of great significance for future developments. As examples, we recall among the others the possible improvements of ultrasound imaging [11, 12], the action of ablation, denaturation or emulsification of ill or damaged tissues[11, 13] when high intensity focused ultrasound are employed, the overcoming of the blood-brain barrier[14]. Even in the engineering field it is impossible to take into account all the growing applications of cavitation (here are just a few references [15–18]).

At the basis of the description of bubble dynamics there are many assumptions introduced in order to make the analytical study or, more frequently, the numerical integration of the model feasible. First of all, in many contexts bubbles are ideally described as spherical: this hypothesis is reasonable when a spherical symmetry of the physical conditions is present, when the bubble is immersed in a liquid that is not too viscous, when it is far from other possible bubbles and from vessel's walls, when its dimensions are sufficiently small and the amplitude of the acoustic forcing not too high. Under these hypotheses it is possible to make use of equations that describe the oscillation of the bubble radius R, among these we recall, for example, the Rayleigh Plesset [19] and the Keller Miksis[20] ones. The laws that rule R obviously depend both on the nature of the liquid in which the bubble is immersed and on the dynamics of the gas. Since bubbles are often objects with dimensions of the order of a few or a few tens of micrometers, it is not easy to have precise experimental data on the physical quantities that characterize the thermodynamic behaviour of the gas contained in them: temperature, mass density and pressure are usually not known with precision inside the bubble. For this reason, the aspects related to gas modelling are particularly delicate: only the overall behaviour of the bubble or the presence of oscillations with different frequencies can be easily observed by images or analysis of the sound signal. For the sake of simplicity, the pressure of the gas in the interface with the liquid is frequently modelled as inversely proportional to a power of the radius of the bubble itself, introducing an exponent proportional to the so-called polytropic index (this index is set equal to 1 in the case of an isothermal phenomenon, while it coincides with the specific heat ratio in the adiabatic case)[5, 7, 9, 21, 22]. Through this simplification of the problem the radius equation is self-consistent and can be integrated on its own. Another approach is to provide a more accurate description of the phenomena that take place inside the bubble by coupling the Rayleigh Plesset or the Keller Miksis equation to a set of partial differential equations (PDEs) or ordinary differential equations (ODEs) that take into account the details[23–26]. This second strategy provides more precise results, but it is also much more expensive from the point of view of numerical calculation. Even in this case, however, some simplifications are necessary: many authors refer to the hyperbolic conservation laws for an Euler gas to describe the gas dynamics[25], ignoring the effects associated with heat conductivity and viscosity; others use the parabolic model of Navier-Stokes Fourier (NSF) approximations, but neglect the effects of viscosity[23, 24, 26]. Subsequently, it was verified that the wide temperature variation observable in regimes such as sonoluminescence necessarily requires not neglecting the thermal effects and the heat exchange between the gas and the liquid[6, 10, 26, 27]. In all

* Electronic mail: leonardo.seccia@unibo.it

cases the presence of gas bulk viscosity and dynamic pressure is not contemplated. This fact is not surprising: on the one hand, Stokes' hypothesis has led several authors in the past to consider the effects linked to dynamic pressure irrelevant, on the other hand the difficulties linked to the measurement of bulk viscosity and the very few experimental data available (often contrasting with each other) make researchers wary of this quantity. Recently, however, it has been shown how dynamic pressure can play a leading role in phenomena related to polyatomic gases: think for instance of shock waves and shock structures also in gas mixtures[28–30], stationary heat conduction[31, 32], dispersion relation of sound[33] and nozzle flow[34]. Moreover, it is worth underlining that the effects of bulk viscosity in fluid dynamics have been the subject of study in situations like turbulent flows[35], hypersonic boundary layers[36] and Rayleigh Taylor instability[37]. In addition to the growing interest in the phenomena related to bulk viscosity, possible high values of this quantity are reported in the literature for some gases such as carbon dioxide (CO_2). Given the ever-increasing number of articles dealing with micro- or nano-bubbles of CO_2 and other polyatomic gases in geophysical, environmental, industrial, engineering, medical fields (to quote just few references[38–43]), it is natural to wonder if bulk viscosity and dynamic pressure could affect bubble dynamics. To our knowledge there is currently no answer to this question in the literature.

In this preliminary work we try to verify whether there is an effect of dynamic pressure on the behaviour of oscillating bubbles immersed in a liquid and what it can be. For this purpose it is mandatory to refer to a gas model that takes into account the presence of this quantity. We have already shown[44] how in the adiabatic limit the Navier approximation for the dynamic pressure could predict excessive effects on the radius of the bubble, resulting equivalent to a significant variation of the liquid viscosity (such an effect was already shown to be inconsistent with available experimental data[9, 23]). For this reason in what follows we refer to the theory of Rational Extended Thermodynamics (RET).

RET was introduced to describe behaviour of a gas in conditions far from thermodynamic equilibrium and in the past it has proven to be able to predict phenomena that classical thermodynamics is unable to describe accurately (shock waves and shock structures, light scattering, dispersion of sound, etc.)[45, 46]. Its peculiarity (from which the name also derives) consists in extending the number of field variables considered independent, adding to the usual mass density, momentum and equilibrium pressure (or temperature) also the heat flux, the dynamic pressure etc. It is therefore natural to ask whether a RET theory is able to predict further phenomena inside the bubble and whether these phenomena give significant effects or can be observable indirectly in an experiment.

As already mentioned, in [44] we investigated whether the dynamic pressure could influence the behaviour of the gas bubble immersed in a liquid and subjected to a periodic forcing, showing that on very short time scales a high bulk viscosity can have a stabilizing effect, reducing the possibility of shock wave formation. In [44] we have also observed that the deviatoric part of the stress tensor is usually negligible. For this reason, in what follows we will neglect the effect of deviatoric part of the stress tensor and shear viscosity. The balance laws that we will employ for the gas dynamics are therefore obtained from the 14-moment RET for a polyatomic gas, imposing the deviatoric part of the stress tensor to be zero. They will be compared with other sets of equations known in the literature, in the case of a gas with a high bulk viscosity. We will then proceed to the construction of the homobaric model. In fact, the idea that the gas pressure is spatially homogeneous is commonly accepted by the scientific community [2, 7, 9, 10, 24, 47], at least when there is no violent shrinkage[8, 48].

Moreover, the equations will be further simplified to obtain a system of easily treatable ODEs in the case of long time numerical integrations.

In this regard, it should be recalled that a RET description of the bubble gas provides for the presence of different time scales associated with the inverse of the angular frequency, ω, of the acoustic forcing, with the time taken by a signal to move from the centre to the boundary of the bubble, with the relaxation times of heat flux and dynamic pressure. It will be precisely the different ratios between these time scales that give rise to peculiar effects and decide which are the most relevant aspects observable at a macroscopic level.

The article is structured as follows. After the introduction contained in section I, we move on to a brief presentation of the physics of the problem and of the state of the art about the bubble dynamics. Sections III and IV provide the main information on the RET theories and introduces the main ideas of the model construction. The validity of the homobaric assumption is tested in section V, where the concept of generalized polytropic index is also introduced. This section includes a comparison between the results obtained from the RET model and what is already known in the literature. In section VI, the homobaric model is derived, tested and validated. Section VII contains the preliminary numerical results also on long integration times, obtained thanks to a further hypothesis on the polynomial trend of temperature and heat flux. Finally, the conclusions can be found in the last section.

II. THE BEHAVIOUR OF A GAS BUBBLE IN A LIQUID

A gas bubble in a liquid is among the simplest examples of multiphase systems. It is usually generated by mechanical, optical or acoustic devices. The bubble can be an ephemeral entity that dissolves in a very short time, as in the case of unstable bubbles due to their too small or too large size. Under appropriate physical conditions, however, it is also possible to obtain bubbles that remain suspended in an acoustic trap[49] for very long intervals (compared to the time scales involved) and that can be studied by high speed imaging and acoustical techniques [8, 9]. Frequently the scenario that presents itself is not that of a single or isolated bubble, but of a multi-bubble fluid. However, it is important to start from the study of the single bubble, seen as a very simple but complete prototype. The presence of a periodic acoustic signal gives rise to a periodic pressure wave in the liquid associated with cavitation and

oscillation of existing bubbles. Being able to model with detail and precision all the phenomena associated with this type of effect is a very important but complicated challenge, for the reasons we have already listed in the introduction.

Depending on the environment in which they are suspended, the technique with which they were generated and the stresses to which they are subjected, bubbles can take very different shapes. Of all the shapes, the spherical one is the most stable and studied, given the mathematical simplicity with which it is possible to represent it. In that case, in fact, it is sufficient to predict the behaviour of the radius as time varies to have a complete picture of the bubble dynamics. Over the decades, many models have been introduced and improved in order to understand and mathematically describe all the peculiar effects associated with bubbles.

A first model, commonly called Rayleigh-Plesset equation, was introduced by Rayleigh[1] and then improved by Plesset [19, 50]: we write it (neglecting the vapour effect) as

$$R\ddot{R}+\frac{3}{2}\dot{R}^2=\frac{1}{\rho_L}\left[p_g(R,t)-p_0-p_a(t)-\frac{2\sigma_L}{R}-\frac{4\mu_L\dot{R}}{R}\right], \tag{1}$$

if ρ_L denotes the liquid mass density, p_0 the ambient pressure, $p_g(r,t)$ the pressure of the gas inside the bubble depending on the radial coordinate r, $p_a(t)$ represents the acoustic driving pressure (for example $p_a=P_{a0}\sin(\omega t)$), while σ_L and μ_L indicate respectively the surface tension and the liquid viscosity. In this case the liquid is assumed to be incompressible.

A few years later, Gilmore[51] proposed a new equation for R that takes into account the sound radiation of the bubbles in the liquid. In the 1980s Keller and Miksis[20] incorporated in the model both the effects analysed by Gilmore and a delay. This last equation is not simple to handle and it is often linearized with respect to the parameter $1/c_L$ (where c_L is the sound speed of the liquid) giving rise to the expression that from now on we will call approximated Keller Miksis equation[9]:

$$\begin{aligned}&\left(1-\frac{\dot{R}}{c_L}\right)R\ddot{R}+\frac{3}{2}\left(1-\frac{\dot{R}}{3c_L}\right)\dot{R}^2=\\&=\left(1+\frac{\dot{R}}{c_L}\right)\frac{1}{\rho_L}p_l+\frac{R}{\rho_L c_L}\frac{dp_l}{dt},\\&\text{with }\ p_l=\left[p_g(R,t)-p_0-p_a(t)-\frac{2\sigma_L}{R}-\frac{4\mu_L\dot{R}}{R}\right].\end{aligned} \tag{2}$$

Since then other equations have been proposed, among them we mention for example the model[2] of the 90s up to the very recent work in [52].

In what follows we will focus on (1) and (2). These are ordinary differential equations that show the same mathematical structure as a damped and forced nonlinear oscillator, and therefore they also present the same phenomena: small amplitude oscillations, transients, asymptotic solutions, resonances, highly non-linear behaviours, deterministic chaos [3, 9, 21, 23]. In particular, given the non-linearity, it will not be possible to determine analytical solutions for these ODEs, unless the bubble is a gas-free cavity. In this regard, as already announced in the introduction, one faces the problem of closing equation (1) or (2), since knowledge of the gas pressure is required in order to proceed with the integration. To obtain a simple model, p_g can be assigned as a power of R or the system that rules the gas dynamics can be coupled to the law for the radius.

To carry out explicit calculations in the next sections we will always assume that the liquid around the bubble is water. For convenience we recall here the main physical parameters of H_2O at room temperature required by the models (including thermal conductivity k_L):

$$\begin{aligned}&\rho_L=10^3\ \text{Kg/m}^3,\quad c_L=1481\ \text{m/s},\quad \sigma_L=0.0728\ \text{N},\\&\mu_L=10^{-3}\ \text{Pa s},\quad k_L=0.598\ \text{W/(K m)},\quad p_0=10^5\ \text{Pa};\end{aligned} \tag{3}$$

we will prescribe the same values at 300 K temperature as well.

III. A QUICK LOOK TO THE THEORIES OF RATIONAL EXTENDED THERMODYNAMICS

As already mentioned, RET was introduced by Müller, Ruggeri and others [45] with the aim of describing non-equilibrium physical phenomena through a system of balance laws that can be written in hyperbolic symmetric form with convex entropy. The hyperbolic nature of the equations allows to overcome the age-old paradox of infinite speed typical of parabolic systems[45] and turns out to be particularly useful in the case of very rapid changes or in the presence of multiple time scales. More than 10 years ago, the theory, first introduced for monatomic gases, was developed for polyatomic ones, by Arima, Taniguchi, Ruggeri and Sugiyama [46, 53]. To write the equations of a RET theory different approaches may be followed: one can either work at a phenomenological level by requiring the validity of the fundamental principles (Galilean invariance, entropy etc.)[45, 53], or derive the equations from the Boltzmann equation through the method of moments[45, 46], constructing infinite hierarchies of moments which are then truncated and closed. In the case of a polyatomic gas the number of hierarchies must be at least two[46, 54] and the distribution function $f=f(t,\mathbf{z},\mathbf{c},I)$, which appears as unknown in Boltzmann equation, must necessarily take into account a scalar variable I that represents the internal molecular modes. In addition, f depends on the usual variables: microscopic velocity $\mathbf{c}=(c_1,c_2,c_3)$, time t and Cartesian spatial coordinates $\mathbf{z}=(z_1,z_2,z_3)$[55]. The densities ($\mathbf{F}$ and $\mathbf{G}$) and the fluxes ($\mathbf{F}^l$ and $\mathbf{G}^l$) of the two hierarchies[46] are defined respectively in following way

$$\begin{aligned}&\mathbf{F}=(F,F_{s_1},F_{s_1s_2},F_{s_1s_2s_3},F_{s_1s_2s_3s_4},\dots)^T,\\&\mathbf{F}^l=(F_l,F_{ls_1},F_{ls_1s_2},F_{ls_1s_2s_3},F_{ls_1s_2s_3s_4},\dots)^T,\\&\mathbf{G}_{ss}=(G_{ss},G_{sss_1},G_{sss_1s_2},G_{sss_1s_2s_3},G_{sss_1s_2s_3s_4},\dots)^T,\\&\mathbf{G}^l_{ss}=(G_{lss},G_{lsss_1},G_{lsss_1s_2},G_{lsss_1s_2s_3},G_{lsss_1s_2s_3s_4},\dots)^T,\end{aligned}$$

if all the integer indexes l, s and s_k with $k\in\mathbb{N}\backslash\{0\}$ vary from 1 to 3 and the convention holds that a repeated index is assumed to be summed on all the values it can take on. The

moments are in turn defined starting from the integration of the distribution function as ($n,k \in \mathbb{N}\backslash\{0\}$)

$$
\begin{aligned}
&F = m\iiint_{\mathbb{R}^3}\int_0^\infty f\varphi(I)dId\mathbf{c},\\
&F_{s_1s_2\ldots s_n} = m\iiint_{\mathbb{R}^3}\int_0^\infty fc_{s_1}c_{s_2}\ldots c_{s_n}\varphi(I)dId\mathbf{c},\\
&G_{ss} = m\iiint_{\mathbb{R}^3}\int_0^\infty f\left(c^2+2I/m\right)\varphi(I)dId\mathbf{c},\\
&G_{sss_1s_2\ldots s_k} = m\iiint_{\mathbb{R}^3}\int_0^\infty f(c^2+2I/m)c_{s_1}c_{s_2}\ldots c_{s_k}\varphi(I)dId\mathbf{c},
\end{aligned}
$$

where m is the molecular mass of the gas, $\varphi(I)$ denotes the weighting measure which is fixed based on the equilibrium caloric equation of state of the polyatomic gas. Thus, the structure of the two infinite hierarchies deduced from the Boltzmann equation can be summarized as[46]

$$
\partial_t\mathbf{F}+\partial_{z_l}\mathbf{F}^l=\mathbf{P},\quad \partial_t\mathbf{G}_{ss}+\partial_{z_l}\mathbf{G}^l_{ss}=\mathbf{Q},
$$

if $\partial_t=\partial/\partial t$ and $\partial_{z_l}=\partial/\partial z_l$. Moreover, $\mathbf{P}$ and $\mathbf{Q}$ are the production terms of the balance laws deduced from the collisional terms of the Boltzamnn equation through the moment method, so that

$$
\begin{aligned}
&\mathbf{P}=(0,0_{s_1},P_{s_1s_2},P_{s_1s_2s_3},\ldots)^T\\
&\mathbf{Q}=(0,Q_{sss_1},Q_{sss_1s_2},Q_{sss_1s_2s_3},\ldots)^T,
\end{aligned}
$$

where the vanishing components correspond to the conservation laws of mass, momentum and energy.

By truncating the hierarchies at a fixed number of moments, the problem of how to express the last flux and the production terms as a function of the independent field variables arises. For this purpose, the Maximum Entropy Principle is commonly used[45, 46]. One of the most well-known and used polyatomic gas models for applications is the 14 moment one, usually indicated as $\mathrm{ET}_{14,P}$ (where the subscript P indicates the fact that the gas is polyatomic)[46, 53]. In this case the 14 independent field variables include the mass density of the gas ρ, the macroscopic velocity $\mathbf{v}$, the equilibrium pressure p, the dynamic pressure Π, the deviatoric part of the stress tensor $\sigma_{\langle ij\rangle}$ $(i,j=1,2,3)$ and the heat flux $\mathbf{q}=(q_1,q_2,q_3)$. The theory is obtained by truncating $\mathbf{F}=(F,F_{s_1},F_{s_1s_2})$ and $\mathbf{G}_{ss}=(G_{ss},G_{sss_1})$. Thanks to the Maximum Entropy Principle, one deduces a system of equations in perfect agreement with that obtained on a phenomenological level[46]. It should also be reminded that in the limit of a polyatomic gas that becomes monatomic the theory tends towards the well-known Grad's system of 13 equations[46].

For the sake of simplicity, from now on we will assume the gas to be ideal and polytropic, that is to say

$$
p=\frac{k_B\rho T}{m},\qquad \mathrm{e}=c_VT=\frac{k_BDT}{2m},\tag{4}
$$

where k_B represents the Boltzmann constant, e indicates the specific internal energy, c_V denotes the specific heat at constant volume, D is the number of molecular degrees of freedom of the gas ($D=3$ in a monoatomic gas and $D>3$ for a polyatomic one). In this case it was proven[46] that $\varphi(I)=I^{(D-5)/2}$. After several mathematical steps and some additional assumptions to simplify the calculations and overcome convergence problems[46], one obtains the 14-moment system approximated in a neighbourhood of an equilibrium state through an expansion in the non-equilibrium fields. In the case of a linear expansion, the equations can be written in Cartesian coordinates as[46]

$$
\begin{aligned}
&\partial_t\rho+\partial_{z_l}(\rho v_l)=0,\\
&\partial_t(\rho v_j)+\partial_{z_l}(\rho v_iv_l+(p+\Pi)\delta_{il}-\sigma_{\langle il\rangle})=0,\\
&\partial_t(\rho v^2+2c_V\rho T)+\partial_{z_l}[(\rho v^2v_l+2(c_V\rho T+p+\Pi)v_k-\\
&-2\sigma_{\langle il\rangle}v_l+2q_k]=0,\\
&\partial_t(\rho v_iv_j+(p+\Pi)\delta_{ij}-\sigma_{\langle ij\rangle})+\partial_{z_l}[\rho v_iv_jv_l+\\
&+(p+\Pi)(v_i\delta_{jl}+v_j\delta_{il}+v_l\delta_{ij})-\sigma_{\langle ij\rangle}v_l-\sigma_{\langle il\rangle}v_j\\
&-\sigma_{\langle jl\rangle}v_i+\frac{2}{D+2}(q_i\delta_{jl}+q_j\delta_{il}+q_l\delta_{ij})]=\\
&=-\frac{\Pi\delta_{ij}}{\tau_\Pi}+\frac{\sigma_{\langle ij\rangle}}{\tau_\sigma},
\end{aligned}
\tag{5}
$$

$$
\begin{aligned}
&\partial_t(\rho v^2v_i+2(c_V\rho T+p+\Pi)v_i-2\sigma_{\langle il\rangle}v_l+2q_i)+\\
&+\partial_{z_l}[\rho v^2v_iv_l+2c_v\rho Tv_iv_l+(p+\Pi)(v^2\delta_{il}+4v_iv_l)-\\
&-\sigma_{\langle il\rangle}v^2-2\sigma_{\langle ij\rangle}v_lv_j-2\sigma_{\langle lj\rangle}v_iv_j+\frac{4}{D+2}q_jv_j\delta_{il}+\\
&+\frac{2(D+4)}{D+2}(q_iv_l+q_lv_i)+\frac{p}{\rho}((D+2)p+(D+4)\Pi)\delta_{il}-\\
&-\frac{p}{\rho}(D+4)\sigma_{\langle il\rangle}]=-\frac{2q_i}{\tau_q}-2\left(\frac{\Pi\delta_{il}}{\tau_\Pi}-\frac{\sigma_{\langle il\rangle}}{\tau_\sigma}\right),
\end{aligned}
$$

where the first three equations correspond to the conservation laws for mass, momentum and energy of a polytropic ideal gas, while the remaining balance laws contain relaxations terms. The relaxation times τ_σ, τ_q and τ_Π are associated with non equilibrium variables: deviatoric part of the stress tensor, dynamic pressure and heat flux. The set (5) turns out to be of hyperbolic type at least in a region of the phase space called hyperbolicity region, which contains the equilibrium state [56].

Since in this work the attention is focused on dynamic pressure, it is useful here to recall its physical meaning and the role it plays in the study of gas dynamics. As demonstrated with a comparison between different kinetic approaches in[57], to which we refer for more details, the onset of the dynamic pressure can be roughly described in two equivalent ways: firstly, it is linked to the energy exchange between the translational and the internal degrees of freedom of the molecule in a non-equilibrium state (hence the idea that it is not observable in a monatomic gas, where internal modes are not present); secondly, the dynamic pressure can be expressed as the difference of pressure between equilibrium and non-equilibrium states.

A quantity of this kind comes into play in the dynamics of bubbles, thought of as devices that periodically restore non-equilibrium conditions during oscillation without allowing a complete relaxation of the system, at least for bubbles that are not too large and for sufficiently small oscillation periods.

As already repeated, in the case of RET the dynamic pressure constitutes an independent field variable like pressure or mass density, but already in the classical thermodynamics of continuous media the stress tensor is usually decomposed into the isotropic and the deviatoric part as

$$t_{ij} = -(p+\Pi)\delta_{ij} + \sigma_{\langle ij\rangle}, \qquad i,j = 1,2,3,$$

where δ_{ij} is the Kronecker symbol, p the equilibrium or thermodynamic pressure, while Π is precisely $-1/3$ of the trace of the viscous tensor, σ_{ij}. The sum $p+\Pi$ is commonly called total pressure. Under the conditions of Navier-Stokes approximation, it is possible to derive a constitutive relation for the dynamic pressure[46, 57, 58], similar to that of $\sigma_{\langle ij\rangle}$, that is:

$$\Pi_{NS} = -\mu_b \frac{\partial v_l}{\partial z_l},$$

which in the isothermal or adiabatic limit in spherical symmetry gives $\Pi = -3\mu_b \dot{R}/R$, overestimating its contribution in the case of high values of bulk viscosity[44].

IV. SIMPLIFIED EQUATIONS FOR A GAS BUBBLE DEDUCED FROM RET

While on the one hand $\mathrm{ET}_{14,P}$ equations constitute an excellent starting point to describe the aspects of gas dynamics that we wish to investigate (heat flux and dynamic pressure in particular), on the other hand they represent a complicated set of balance laws if a bounded domain variable in time is taken into account. In[44, 59] we have already highlighted the advantages of using this model for very short time intervals. However, the oscillating gas bubble scenario is much more varied and complex and many phenomena require very time-consuming integrations.

The first step towards reducing and simplifying the system is to focus on the deviatoric part of the stress tensor. This quantity is always neglected in bubble literature and is bound to vanish in adiabatic conditions[44]. Even in the Navier-Stokes approximation, it is clear that the deviatoric part of the stress tensor is zero for a perfectly spherical symmetry and for radial components of heat flux and velocity linear in the radial coordinate r, but this is not true for Π. If, on the contrary, we face a non-linear dependence of velocity and heat flux on r, but the homobaricity conditions hold, the structure of $\mathrm{ET}_{14,P}$ implies that $\sigma_{\langle ij\rangle}$ is at least some orders of magnitude lower than dynamic pressure and heat flux.

Therefore, from now on we will neglect in sytem (5) the deviatoric part of the stress tensor and its corresponding equation. After deducing the homobaric model in section VI, it would be possible to verify a posteriori the reasonableness of this assumption, proving it to be correct within the range of validity of the homobaric hypothesis.

Introducing the material derivative ($d/dt = \partial_t + \mathbf{v}\cdot\nabla$) and assuming $\sigma_{\langle ij\rangle}$ to be negligible, the field equations (5) reduce to

$$\begin{aligned}
&\frac{d\rho}{dt} + \rho\nabla\cdot\mathbf{v} = 0,\\
&\rho\frac{d\mathbf{v}}{dt} + \nabla(p+\Pi) = 0,\\
&\frac{D}{2}\frac{dp}{dt} + \left(\frac{D+2}{2}p+\Pi\right)\nabla\cdot\mathbf{v} + \nabla\cdot\mathbf{q} = 0,\\
&\frac{d\Pi}{dt} + \left(\frac{2(D-3)}{3D}p + \frac{5D-6}{3D}\Pi\right)\nabla\cdot\mathbf{v} +\\
&+ \frac{4(D-3)}{3D(D+2)}\nabla\cdot\mathbf{q} = -\frac{1}{\tau_\Pi}\Pi,\\
&\frac{d\mathbf{q}}{dt} + \frac{D+4}{D+2}(\mathbf{q}\nabla\cdot\mathbf{v} + \mathbf{q}\cdot\nabla\mathbf{v}) + \frac{2}{D+2}(\nabla\otimes\mathbf{v})\mathbf{q} -\\
&- \frac{p}{\rho}\nabla p + \frac{p}{2\rho T}\nabla T + \frac{p-\Pi}{\rho}\nabla(p+\Pi) = -\frac{1}{\tau_q}\mathbf{q}.
\end{aligned} \tag{6}$$

Referring to[46, 53], the relaxation times are phenomenologically defined as

$$\tau_\Pi = \frac{3D\mu_b}{2(D-3)p}, \qquad \tau_q = \frac{2k_g m}{(D+2)k_B p}, \tag{7}$$

if μ_b and k_g denotes the bulk viscosity and the heat conductivity of the gas. While k_g has been widely studied in the literature and there is complete agreement on its values, bulk viscosity is currently little-studied with respect to shear viscosity, μ_s[60]; moreover, very different values are reported for the same substance and for the same physical conditions. This fact is particularly true for gases like CO_2. Let us recall, for example, that for CO_2 gas at room temperature the ratio between the bulk and the shear viscosity ($r_\mu = \mu_b/\mu_s$) has been the subject of extensive scientific discussion and values ranging from about 1 to 4000 are reported in literature[29, 61–63]. The reason behind these apparently surprising results is the variety of experimental techniques employed, that is, in particular, absorption and dispersion of sound waves (at MHz frequencies) and Rayleigh-Brillouin scattering (at GHz frequencies). In fact, for polyatomic gases, as CO_2, the primary cause of bulk viscosity is the finite rate of energy exchange between translational and internal (rotational and vibrational) degrees of freedoms. Since it is well known that the relaxation time of vibrational energy is much longer than that of rotational energy (e.g. for CO_2 one has 6×10^3 ns versus 0.30 ns) [64], when μ_b is measured at MHz frequencies both rotational and vibrational degrees of freedom are active, while at GHz frequencies only the rotational ones remain, given that the vibrational degrees are frozen[65].

It is convenient to write the previous equations in spherical coordinates under the following two hypotheses: 1) all the field variables depend only on the radial coordinate r (where, as usual, $r = 0$ corresponds to the centre of the bubble) and not on the angles, so that it is guaranteed that the shape remains spherical as time varies; 2) the perfect radial symmetry implies that heat flux and velocity have only a radial component.

So, the system (6) reduces to

$$\begin{aligned}
&\partial_t\rho+\frac{1}{r^2}\partial_r(r^2\rho v)=0,\\
&\partial_t v+v\partial_r v+\frac{1}{\rho}\partial_r(p+\Pi)=0,\\
&\partial_t p+\frac{1}{r^2}\partial_r(r^2pv)+\frac{2}{D}(p+\Pi)\frac{1}{r^2}\partial_r(r^2v)+\frac{2}{D}\frac{1}{r^2}\partial_r(r^2q)=0,\\
&\partial_t\Pi+\frac{1}{r^2}\partial_r(r^2\Pi v)+\frac{2(D-3)(p+\Pi)}{3Dr^2}\partial_r(r^2v)+\\
&+\frac{4(D-3)}{3D(D+2)r^2}\partial_r(r^2q)=-\frac{\Pi}{\tau_\Pi},\\
&\partial_t q+\frac{1}{r^2}\partial_r(r^2qv)+\frac{2q}{(D+2)r^2}\partial_r(r^2v)+\frac{D+6}{D+2}q\partial_r v+\\
&+\frac{p}{\rho T}\left[\frac{(D+2)(p+\Pi)+2\Pi}{2}\right]\partial_r T-\frac{\Pi}{\rho}\partial_r(p+\Pi)+\\
&+\frac{p}{\rho}\partial_r\Pi=-\frac{q}{\tau_q},
\end{aligned}\tag{8}$$

where for the sake of brevity v and q from now on represent the radial component of velocity and heat flux.

In the next sections, to present some particular cases and construct exemplary figures, we will refer specifically to CO_2 gas. We hereby indicate the main physical parameters[66] required by the simulations at $T=300$ K:

$$\begin{aligned}
&m=7\times10^{-26}\text{ Kg},\quad k_g=16.8\times10^{-3}\text{ W/(K m)},\\
&\mu_s=15\times10^{-6}\text{ Pa s},\quad r_\mu\in[1,2000],\quad D=7.
\end{aligned}\tag{9}$$

Regarding the value assigned to the D parameter it should be reminded that identifying the degrees of freedom of a gas molecule could sometimes be a delicate matter. In fact, it is necessary to consider the temperature dependence of the degrees of freedom [66, 67], especially with regard to vibrational ones, that must be multiplied by two, since a vibrational mode involves both potential and kinetic energy. In particular, for CO_2 at $T=300$K one has the number of 6.83[66]. In a non-polytropic gas model this value varies as temperatures vary. Since we limit our analysis to a polytropic approximation of the gas, we have chosen the integer value of D equal to 7, deferring to subsequent studies a more realistic description of the dependence of specific heats on temperature. CO_2 gas is also known to present peculiarities in the phenomena of cavitation and sonoluminescence[68, 69], thus representing an excellent candidate for the in-depth study of the role of dynamic pressure.

As already stated in the introduction, four different time scales implicitly appear in this system of equations: the two relaxation times τ_q e τ_Π, the oscillation time of the bubble radius proportional to $t_\omega=\omega^{-1}$ and finally the propagation time of a signal from the boundary to the centre of the bubble at equilibrium, that is proportional to $t_0=R_0/\sqrt{k_BT_0/m}$, if T_0 denotes the initial temperature of the gas and R_0 the equilibrium radius. To introduce dimensionless field variables it is advisable to refer to the time scale associated with the acoustic pressure, t_ω, and to the spatial scale given by R_0, so that

$$\begin{aligned}
&t=\omega^{-1}\hat{t},\quad r=R_0\hat{r},\quad \rho=\rho_0\hat{\rho},\quad v=R_0\omega\hat{v},\\
&T=T_0\hat{T},\quad p=p_g^E\hat{p},\quad \Pi=p_g^E\hat{\Pi},\quad q=p_g^ER_0\omega\hat{q},
\end{aligned}\tag{10}$$

if ρ_0 is the initial mass density of the gas and $p_g^E=k_B\rho_0T_0/m$ denotes the initial equilibrium total pressure (in the absence of a driving pressure). Thus, equation $(8)_2$ becomes

$$r_t^2(\partial_{\hat{t}}\hat{v}+\hat{v}\partial_{\hat{r}}\hat{v})+\frac{1}{\hat{\rho}}\partial_{\hat{r}}(\hat{p}+\hat{\Pi})=0,\text{ if }r_t^2=\frac{R_0^2\omega^2\rho_0}{p_g^E},\tag{11}$$

and it is clear that if the ratio $r_t^2=t_0^2/t_\omega^2$ is sufficiently small, the total pressure $p+\Pi$ is approximately homogeneous in space (homobaric assumption).

V. THE VALIDITY OF THE HOMOBARIC HYPOTHESIS AND THE GENERALIZED POLYTROPIC INDEX

In this section the validity of the homobaric hypothesis for equations (8) is further investigated in the framework of small amplitude oscillations. Reference is made to the techniques used in [23] by Prosperetti: our aim is to test the model and to understand under which conditions the dynamic pressure has to be taken into account.

Starting from the observation that the bubble radius equation corresponds in the first instance to the equation of a damped and forced harmonic oscillator, it is natural to assume that the asymptotic behavior of the field variables is of the oscillatory type with a frequency equal to that of the periodic forcing. Furthermore, from (1) and (2) it is clear that the pressure inside the bubble at equilibrium must be $p_g^E=p_0+2\sigma_L/R_0=p_0(1+w)$ (see [23]). Thus, approximating the bubble radius as $R=R_0(1+X_1)$ and the gas pressure as $p_g=p_g^E+p_0p_{g1}(r,t)$, and referring to the complex representation, equation (2) reduces to

$$\begin{aligned}
&R_0^2\ddot{X}_1=(1+i\frac{\omega R_0}{c_L})\frac{1}{\rho_L}[p_0p_{g1}(R_0,t)-p_0\varepsilon' e^{i\omega t}+\\
&+\frac{2\sigma_L}{R_0}X_1-4\mu_L\dot{X}_1],
\end{aligned}\tag{12}$$

where it is assumed that the acoustic forcing is $P_a(t)=p_0\varepsilon'\exp(i\omega t)$ and that $|X_1|\ll1$, $|\dot{X}_1|\ll1$, $|\ddot{X}_1|\ll1$. After a suitable transient time the effect of the periodic driving will prevail over the elastic force and the damping one, so that $\dot{X}_1=i\omega X_1$, $\ddot{X}_1=-\omega^2X_1$ and if $\alpha=p_0/(R_0^2\rho_L)$ it holds

$$\begin{aligned}
&X_1=\alpha\frac{p_{g1}-\varepsilon' e^{i\omega t}}{\Delta},\\
&\Delta=-\omega^2(1+i\frac{\omega R_0}{c_L})^{-1}+4i\frac{\mu_L\omega}{R_0^2\rho_L}-\frac{2\sigma_L}{R_0^3\rho_L}.
\end{aligned}\tag{13}$$

In correspondence with small bubble oscillations in the neighbourhood of the equilibrium position $R=R_0$, small oscillations of all the field variables will also be observed. In this

way, for quantities that do not vanish at equilibrium, we can write the following linearization

$$\begin{aligned} &p = p_0(1+w+p_1), \quad \rho = \rho_0(1+\rho_1), \\ &T = T_0(1+T_1),\ T_L = T_0(1+\theta_L), \end{aligned} \tag{14}$$

where T_L denotes the temperature of the liquid. Furthermore, for quantities that are zero at equilibrium we introduce the following dimensionless variables

$$\Pi = p_0\Pi_1, \quad v = p_0 V_1/(\omega R_0\rho_0), \quad q = p_0^2 Q_1/(\omega R_0\rho_0). \tag{15}$$

According to what has already been observed, to these assumptions the following hypothesis is added

$$\begin{aligned} &\partial_t\rho_1 = i\omega\rho_1, \quad \partial_t T_1 = i\omega T_1, \quad \partial_t\theta_L = i\omega\theta_L, \\ &\partial_t\Pi_1 = i\omega\Pi_1, \quad \partial_t V_1 = i\omega V_1, \quad \partial_t Q_1 = i\omega Q_1. \end{aligned} \tag{16}$$

Equations (8) are then approximated as

$$\begin{aligned} &i\omega\rho_1 + \frac{p_0}{\omega R_0\rho_0}\frac{1}{r^2}\partial_r(r^2V_1) = 0, \\ &iV_1 + R_0\partial_r(p_1+\Pi_1) = 0, \\ &i\omega p_1 + \frac{p_0(1+w)(D+2)}{D\omega R_0\rho_0 r^2}\partial_r(r^2V_1) + \\ &+ \frac{2p_0}{D\omega R_0\rho_0}\frac{1}{r^2}\partial_r(r^2Q_1) = 0, \\ &i\omega\Pi_1 + \frac{2(D-3)p_0(1+w)}{3D\omega R_0\rho_0 r^2}\partial_r(r^2V_1) + \\ &+ \frac{4(D-3)p_0}{3D(D+2)\omega R_0\rho_0 r^2}\partial_r(r^2Q_1) = -\frac{\Pi_1}{\tau_\Pi}, \\ &iQ_1 + \frac{(D+2)(1+w)^2R_0}{2}\partial_r T_1 + \\ &(1+w)R_0\partial_r\Pi_1 = -\frac{Q_1}{\omega\tau_q}. \end{aligned} \tag{17}$$

System (17) is coupled to the spherical coordinate equation for the liquid temperature in the Fourier approximation. If q_L denotes the heat flux in the liquid in the radial direction, we have

$$\partial_t\theta_L = -\frac{k_L}{\rho_L c_{v,L}}\frac{1}{r^2}\partial_r\left(r^2\partial_r\theta_L\right), \quad q_L = -k_L T_0\partial_r\theta_L, \tag{18}$$

where k_L is the thermal conductivity of the liquid and $c_{v,L}$ its specific heat at constant volume. In the presence of dynamic pressure, it must hold that $p_g = p+\Pi$ and therefore $p_{g1} = p_1+\Pi_1$. Furthermore, the ideality of the gas, implies the linear relationship $T_1 = -\rho_1 + p_1/(1+w)$. After several calculations one gets that

$$\begin{aligned} &\rho_1 = -\frac{p_0}{\omega^2\rho_0}\frac{1}{r^2}\partial_r\left(r^2\partial_r p_{g1}\right), \quad V_1 = iR_0\partial_r p_{g1}, \\ &\Pi_1 = \frac{2(D-3)}{5D-3i(D+2)\hat{\tau}_\Pi^{-1}}p_{g1} = J_\Pi p_{g1}, \\ &Q_1 = \frac{i(D+2)p_0R_0(1+w)^2(2\partial_{rr}^2p_{g1}+r\partial_{rrr}^3p_{g1})}{2\omega^2(1-i\hat{\tau}_q^{-1})\rho_0 r} - \\ &- \frac{i(D+2)R_0(1+w)(-\omega^2r^2\rho_0+2p_0(1+w))\partial_r p_{g1}}{2\omega^2(1-i\hat{\tau}_q^{-1})r^2\rho_0} - \\ &- \frac{iDR_0(1+w)\partial_r\Pi_1}{2(1-i\hat{\tau}_q^{-1})} \end{aligned} \tag{19}$$

if $\hat{\tau}_\Pi = \tau_\Pi\omega$ and $\hat{\tau}_q = \tau_q\omega$. Making a change of variables ($y = r/R_0$), the equation for the total pressure, becomes

$$\begin{aligned} &\partial_{yyyy}^4(yp_{g1}) + a_2\partial_{yy}^2(yp_{g1}) + a_0(yp_{g1}) = 0, \\ &a_0 = \frac{3D(i+\hat{\tau}_\Pi^{-1})(1-i\hat{\tau}_q^{-1})r_t^4}{(5iD+3\hat{\tau}_\Pi^{-1}(D+2))}, \\ &a_2 = \frac{-J_\Pi Dr_t^2}{(D+2)} + (2-i\hat{\tau}_q^{-1})r_t^2. \end{aligned} \tag{20}$$

Although there are differences in the coefficients, the structure of this equation remains the same as that obtained with the NSF approximations [23].

The following usual boundary conditions are then required:

$$\begin{aligned} &V_1|_{r=0} = 0, \quad v|_{r=R_0} = \dot{X}_1R_0, \quad (T_1-\theta_L)|_{r=R_0} = 0, \\ &\theta_L|_{r=\infty} = 0, \quad \left(\frac{p_0^2Q_1}{\omega R_0\rho_0} - k_LT_0\partial_r\theta_L\right)\Big|_{r=R_0} = 0. \end{aligned} \tag{21}$$

Excluding the presence of singularities in the function $p_{g1}(r,t)$ for $r\to 0$ and in that of θ_L for $r\to\infty$, we obtain the explicit solution of the previous equations which presents the same structure as in the case of NSF model:

$$\begin{aligned} &p_{g1} = \varepsilon' e^{i\omega t}\left[B_1\frac{\sinh(\beta_1 y)}{y\sinh(\beta_1)} + B_2\frac{\sinh(\beta_2 y)}{y\sinh(\beta_2)}\right], \\ &\theta_L = \varepsilon'\frac{B_3e^{-\beta_3(y-1)+i\omega t}}{y(1+w)}, \\ &\text{with}\ \ \beta_{1,2} = \frac{1}{2}(-a_2 \pm (a_2^2-4a_0)^{1/2})^{1/2}, \\ &\beta_3 = (1+i)\left(\frac{\omega R_0^2\rho_L c_{v,L}}{2k_L}\right)^{1/2}. \end{aligned} \tag{22}$$

Constant quantities B_k ($k=1,2,3$) are determined using the remaining boundary conditions. In this way one obtains that

$$\begin{aligned} &B_1 = -\frac{\alpha(1+w)[(1-J_\Pi)r_t^2\bar{k}_L + \beta_2^2\bar{k}_L - (1+w)W_2]}{H_B} \\ &B_2 = \frac{\alpha(1+w)[(1-J_\Pi)r_t^2\bar{k}_L + \beta_1^2\bar{k}_L - (1+w)W_1]}{H_B}, \\ &B_3 = \sum_{j=1}^{2} B_j\left(1-J_\Pi+r_t^{-2}\beta_j^2\right), \end{aligned} \tag{23}$$

where for $j = 1,2$

$$\begin{aligned}
&\bar{k}_L = (\beta_3+1)r_t^{-2}\frac{k_L\omega\rho_0 T_0}{p_0^2}, \quad \lambda_j = \beta_j\coth\beta_j - 1,\\
&W_j = \frac{\lambda_j(1+w)((DJ_\Pi - 2 - D) - \beta_j^2(D+2)r_t^{-2})}{2(i+\hat{\tau}_q^{-1})},\\
&H_B = \alpha(1+w)[(\beta_1^2-\beta_2^2)\bar{k}_L - (1+w)(W_1-W_2)]+\\
&+\Delta[-(\beta_1^2\lambda_2 - \beta_2^2\lambda_1)\bar{k}_L r_t^{-2}+\\
&+(\lambda_1-\lambda_2)\bar{k}_L(1-J_\Pi) - r_t^{-2}(1+w)(\lambda_1 W_2 - \lambda_2 W_1)].
\end{aligned} \tag{24}$$

The validity of the homobaricity hypothesis implies that $|\beta_j|$ is sufficiently "small" and this is possible if $|a_2| \ll 1$, this requirement is compatible with the already mentioned $r_t^2 < 1$ condition. In many situations the behaviour of the gas pressure on the bubble's boundary is described in a simplified way as the sum of two terms: a contribution that is inversely proportional to a power of the radius $R(t)$ through an exponent that we could call *generalized polytropic index*, κ_*, and an additional contribution of an effective viscosity so that

$$p_g = p_0(1+w)\left(\frac{R_0}{R(t)}\right)^{3\kappa_*} - 4\mu_*\frac{\dot{R}}{R(t)}. \tag{25}$$

This approach, already described in the introduction, has the advantage of decoupling the Keller Miksis or the Rayleigh Plesset equation from the PDE system for the gas dynamics. By linearizing the previous relationship for small oscillations it must then hold

$$p_{g1}(R_0,t) \simeq -3\kappa_* p_0(1+w)X_1 - 4i\mu_*\omega X_1, \tag{26}$$

and it is easily deduced that

$$\kappa_* = -\frac{1}{3(1+w)}\Re\left(\frac{\Delta(B_1+B_2)}{\alpha(B_1+B_2-1)}\right), \tag{27}$$

where the symbol $\Re$ denotes the real part. Note that κ_* also takes into account the presence of dynamic pressure: that is why we use the adjective "generalized". However, for a monatomic gas ($D = 3$), J_Π vanishes (see (19)) and κ_* is reduced to the polytropic index κ commonly used in the literature[7–9, 24].

Figures 1-3 present a comparison between the polytropic index, κ, determined from the NFS equations[23] (ignoring the dynamic pressure or assuming r_μ to be small) and the generalized polytropic index, κ_* (calculated here for large values of μ_b).

The behaviour of the two indexes is analysed in Figure 1 as the number of the molecular degrees of freedom of the polytropic gas varies, for assigned $\omega = 10^7$ Hz and by setting the physical constants of the gas equal to those of CO_2 (9) and the liquid parameters coincident with (3). As we have already observed in Section IV, the value of D for a CO_2 gas molecule is close to 7 at 300 K. In this first figure we have considered other plausible values for a polyatomic gas, just to explore the role that D plays on the polytropic index. However, in the following figures $D = 7$ will be prescribed instead. In Figure 2

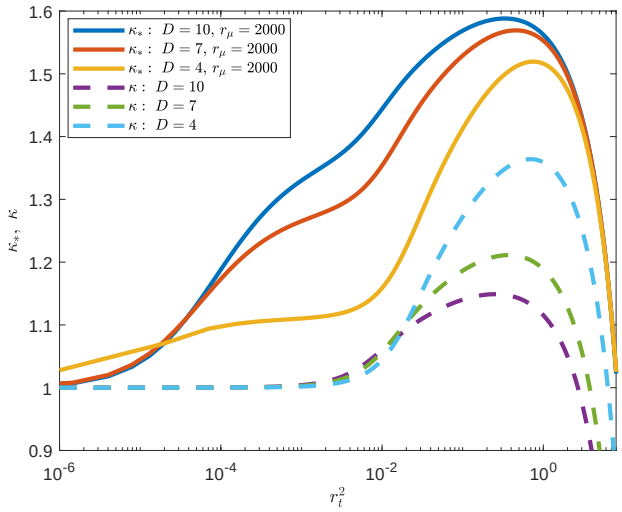

FIG. 1. κ_* and κ compared for different values of the molecular degrees of freedom D.

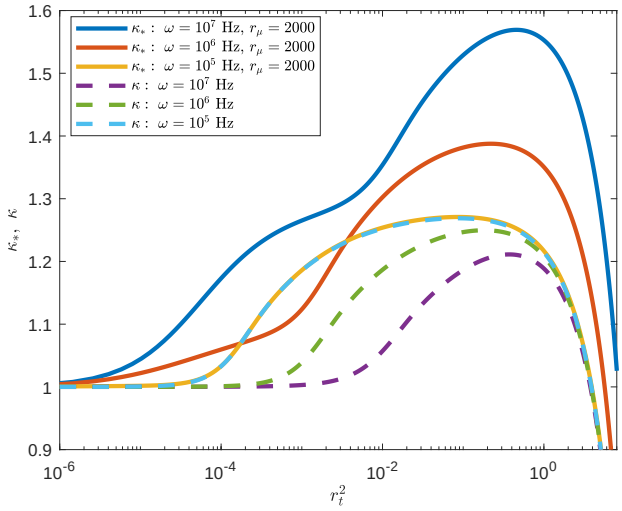

FIG. 2. κ_* and κ compared for different values of the sound angular frequency ω when $D = 7$.

differences between κ and κ_* are observable when different values of ω are assigned. Finally, Figure 3 studies the role of the equilibrium radius, keeping the physical characteristics of gas and liquid unchanged.

VI. A HOMOBARIC MODEL DEDUCED FROM THE RATIONAL EXTENDED THERMODYNAMICS THEORY

To simplify the PDE system (8) coupled with the bubble radius ODE, it is natural to exploit the homobaric hypothesis, following a procedure employed for the Navier Stokes Fourier model without Π, see for example [24]. From the previous section it is also clear that in the range of validity of that hy-

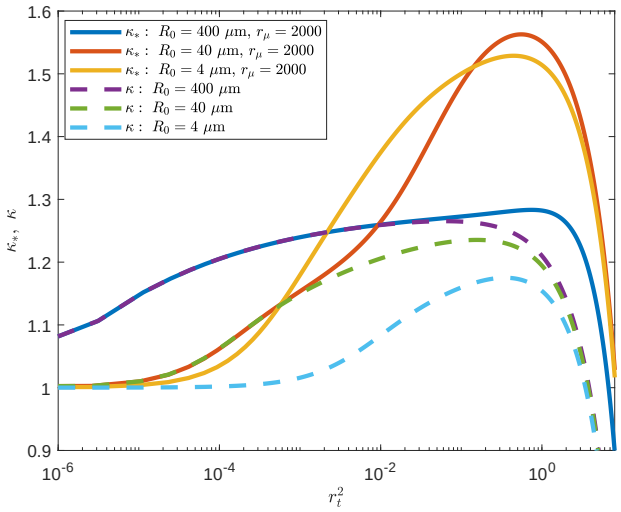

FIG. 3. κ_* and κ compared for different values of the equilibrium radius R_0 when $D = 7$.

pothesis for the total pressure it is correct to consider both the equilibrium pressure and the dynamic one individually homogeneous in space (see equations (19)). By assuming the presence of spherical symmetry, integrating the energy equation $(6)_3$ on a sphere and taking advantage of the divergence theorem, we obtain

$$\frac{Dr}{6}\dot{p} + \left(\frac{D+2}{2}p + \Pi\right)v + q = 0, \tag{28}$$

from which it follows that

$$v = \frac{2}{(D+2)p + 2\Pi}\left[-\frac{Dr}{6}\dot{p} - q\right], \tag{29}$$

if $\partial_r p = 0$ and $\dot{p} = dp/dt$. Moreover, when the sphere coincides with the bubble (i.e. $r = R$), one gets the following ODE ($v|_R = \dot{R}$)

$$\dot{p} = \frac{6}{DR}\left[-\left(\frac{D+2}{2}p + \Pi\right)\dot{R} - q|_R\right]. \tag{30}$$

Through the same steps performed on the balance law of Π, by integrating it on a sphere coincident with the bubble (r=R) we obtain

$$\dot{\Pi} + \frac{4(D-3)}{D(D+2)R}q|_R + \frac{2(D-3)p + (5D-6)\Pi}{D}\frac{\dot{R}}{R} = -\frac{\Pi}{\tau_\Pi}. \tag{31}$$

By considering (29) and the equations for energy and heat flux in spherical coordinates $(8)_{4,5}$, exploiting the ideality of the gas and the homobaric hypothesis for which $T\partial_r\rho + \rho\partial_r T = 0$, and finally introducing the usual change of variables $(t,r) \to (t,x)$ with $x = r/R$[24, 44], the following two hyperbolic PDEs can be deduced:

$$\begin{aligned}
&\partial_t T - 2\frac{q - q|_R x}{((D+2)p + 2\Pi)R}\partial_x T + \frac{2T}{((D+2)p+2\Pi)R}\partial_x q = \\
&= -\frac{6T(p+\Pi)\dot{R}}{DRp} - \frac{4T(Dpq + 3(p+\Pi)q|_R x)}{Dp((D+2)p+2\Pi)Rx}, \\
&\partial_t q + \frac{p((D+2)p + (D+4)\Pi)}{2R\rho T}\partial_x T + \\
&+ \frac{2(-3(D+4)q + (D+2)q|_R x)}{(D+2)((D+2)p+2\Pi)R}\partial_x q = \\
&= \frac{4q((D+4)q - (2D+9)q|_R x)}{(D+2)((D+2)p+2\Pi)Rx} - \frac{q}{\tau_q} - \frac{2(2D+9)\dot{R}q}{(D+2)R}.
\end{aligned} \tag{32}$$

For the sake of simplicity, in the last equations all the terms proportional to q^2, $qq|_R$, $q|_R\partial_x q$ and $q\partial_x q$ can be neglected: they turn out to be of a lower order of magnitude with respect to the remaining terms, as we have verified comparing the results obtained with and without such quadratic terms. The conservation law for the mass of the gas can be replaced, as in [24], by the equivalent integral condition:

$$M_0 = \iiint_{\mathscr{B}} \rho dV = \frac{4\pi R^3 p}{k_B}\int_0^1 x^2 T^{-1} dx, \tag{33}$$

if $M_0 = 4\pi R_0^3 p_0/(3k_B T_0)$ denotes the initial gas total mass inside the bubble $\mathscr{B}$. In this work we assume the conservation of mass inside the bubble, postponing the question of the possible exchange of matter between the bubble and the surrounding liquid to subsequent studies.

A. Small amplitude oscillations

To make a first comparison between the simplified model and equations (8), we start from the hypothesis of small amplitude oscillations and follow the procedure already illustrated in Section V. The aim is to determine the range of validity of these new equations. Referring to (13), (14) and (15), the previous equations are linearized under the assumption of an asymptotic behaviour in time, so that they reduce to (due to previous assumptions $x \simeq y = r/R_0$)

$$\begin{aligned}
&p_1 + \frac{3(D+2)(1+w)}{D}X_1 - \frac{6ir_t^{-2}}{D(1+w)}Q_1|_R = 0, \\
&\Pi_1 + \frac{2(D-3)(1+w)}{D}X_1 - \frac{4i(D-3)r_t^{-2}}{D(D+2)(1+w)}Q_1|_R = i\frac{\Pi_1}{\omega\tau_\Pi}, \\
&T_1 - \frac{2p_1}{(D+2)(1+w)} - \frac{2ir_t^{-2}}{(D+2)(1+w)^2}\partial_x Q_1 = \\
&= \frac{4ir_t^{-2}Q_1}{(D+2)(1+w)^2 x}, \\
&Q_1 - \frac{i(D+2)(1+w)^2}{2}\partial_x T_1 = \frac{iQ_1}{\omega\tau_q}.
\end{aligned} \tag{34}$$

Obtaining p_1, Π_1 and Q_1 from $(34)_{1,2,4}$ and substituting them into the third relation, one gets

$$\partial^2_{yy}(yT_1)+(1-i\hat{\tau}_q^{-1})r_t^2(yT_1)+\frac{2i(i+\hat{\tau}_q^{-1})r_t^2 p_1 y}{(D+2)(1+w)}=0, \quad (35)$$

whose solution (always focusing on the asymptotic behaviour and imposing that $\lim_{y\to 0} Q_1(y)=0$) is

$$\begin{aligned} T_1 &= \left[\frac{2p_1}{(D+2)(1+w)}+C_1\frac{\sinh(\beta_4 y)}{y\sinh\beta_4}\right], \\ \beta_4 &= r_t\sqrt{-1+i\hat{\tau}_q^{-1}}. \end{aligned} \quad (36)$$

The approximated equations (30), (31) and (32) were obtained, requiring that the gas velocity at the boundary ($r=R$) coincide with $\dot{R}$. Thus, in order to determine C_1, one has to consider the remaining conditions regarding temperature and heat flux at the interface gas-liquid (21). To this aim we refer to the model for T_L and q_L presented in (18) and the integration constants C_1 and B_3 turn out to be

$$\begin{aligned} C_1 &= -\frac{4(i+\hat{\tau}_q^{-1})\bar{k}_L p_1}{(D+2)(1+w)(2(i+\hat{\tau}_q^{-1})\bar{k}_L+(D+2)\lambda_4 r_t^{-2}(1+w)^2)}, \\ B_3 &= C_1(1+w)+\frac{2p_1}{D+2}, \\ Q_1|_R &= W_4 p_1(1+w), \quad \lambda_4=\beta_4\coth\beta_4-1 \\ W_4 &= \frac{2\bar{k}_L\lambda_4}{2(i+\hat{\tau}_q^{-1})\bar{k}_L+(D+2)\lambda_4 r_t^{-2}(1+w)^2}, \\ p_1 &= -\frac{3(D+2)(1+w)X_1}{D-6ir_t^{-2}W_4}, \quad \Pi_1=\frac{2i(D-3)}{3(i+\hat{\tau}_\Pi^{-1})(D+2)}p_1. \end{aligned} \quad (37)$$

In this way the generalized polytropic index for this homobaric simplified model turns out to be

$$\kappa_*^h \simeq -\Re\left(\frac{p_1+\Pi_1}{3(1+w)X_1}\right)=\Re\left(\frac{5iD+3\hat{\tau}_\Pi^{-1}(D+2)}{3(i+\hat{\tau}_\Pi^{-1})(D-6ir_t^{-2}W_4)}\right). \quad (38)$$

We remark that alternatively it would be reasonable to impose a simplified condition regarding the interface: if the liquid around the bubble is imagined as an infinite reservoir, the temperature at $r=R$ could be prescribed to be constantly equal to T_0. Ignoring, therefore, the relations for temperature and heat flux of the liquid, we could impose that $T(y=1)=T_0$, i.e. that in the regime of small oscillations $T_1(y=1)=0$. Repeating all the calculations, we would obtain an expression for the generalized index $\bar{\kappa}_*^h$ formally identical to (38), but instead of W_4 we should insert $\bar{W}_4=\lambda_4/(i+\hat{\tau}_q^{-1})$.

In Figures 4 and 5 the behaviour of κ_*^h is shown as the sound angular frequency varies for a fixed equilibrium bubble radius or as R_0 varies for an assigned angular frequency. Two very different values of the viscosity ratio are examined for a CO_2 gas (9) and water liquid (3) at 300 K temperature. Note that for r_μ equal to 1 the effect of the bulk viscosity is completely negligible and the results are in full agreement with the homobaric classical model[24]). In Fig. 4 (where $R_0=100$ μm) it

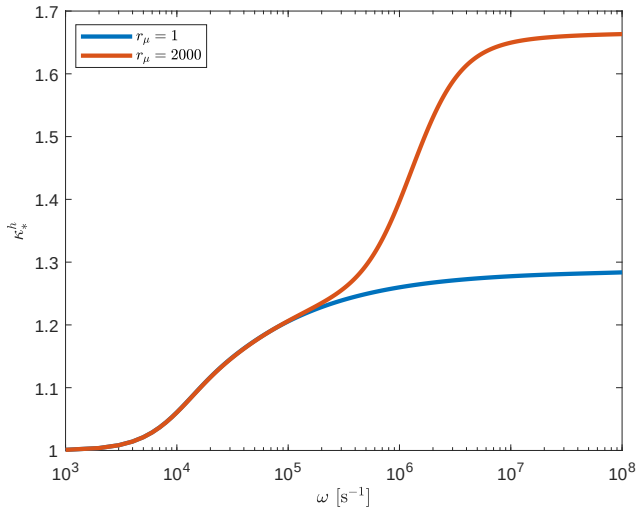

FIG. 4. The behaviour of κ_*^h as a function of ω when R_0 is fixed to be 100 μm, the bubble is filled with CO_2 and immersed in water.

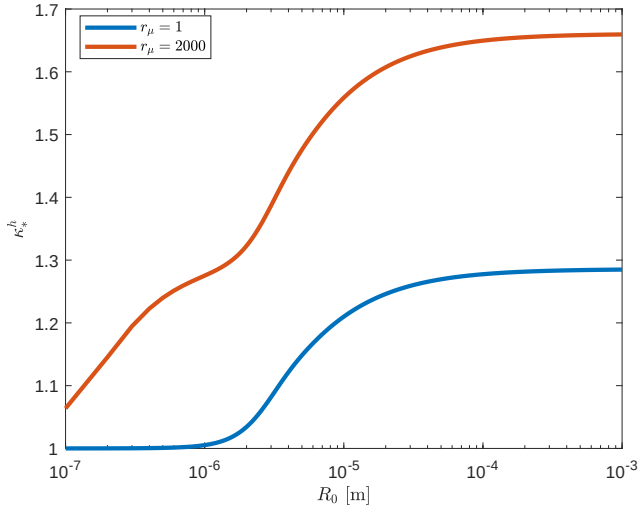

FIG. 5. The behaviour of κ_*^h as a function of R_0 when $\omega=10^7$ Hz, the bubble is filled with CO_2 and immersed in water.

can be seen how small values of the oscillation frequency correspond to the same isothermal behaviour, regardless of the value of μ_b, but as the frequency increases marked differences become visible, and κ_*^h tends to its adiabatic asymptotic value. As we will show in the next sections, this asymptotic value corresponds to γ for "small" r_μ while it tends to 5/3 when $r_\mu \gg 1$. Similar considerations hold in the case of Figure 5 (where $\omega=10^7$ Hz), however for high acoustic frequency, even in an isothermal regime, bulk viscosity could make a difference in bubble dynamics.

Unfortunately, by testing the validity of the homobaric hypothesis it is easily verified that the adiabatic values of the polytropic index are usually not compatible with condition $r_t^2 \ll 1$. Figures 6-11 present the behaviour of κ_*^h as a func-

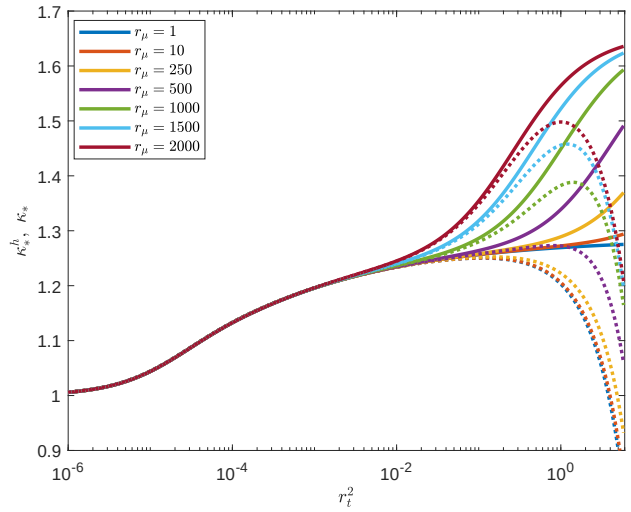

FIG. 6. A comparison between κ_*(dotted line) e κ_*^h (continuous line) as functions of r_t^2, when $R_0 = 100\ \mu$m and different values of r_μ are taken into account.

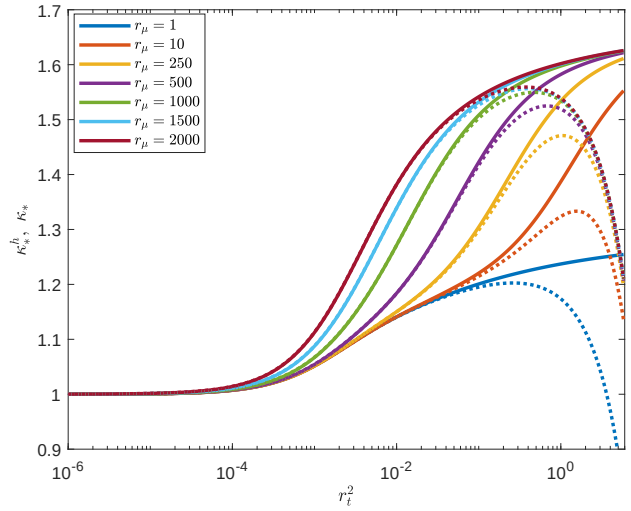

FIG. 7. A comparison between κ_*(dotted line) e κ_*^h (continuous line) as functions of r_t^2, when $R_0 = 10\ \mu$m and different values of r_μ are taken into account.

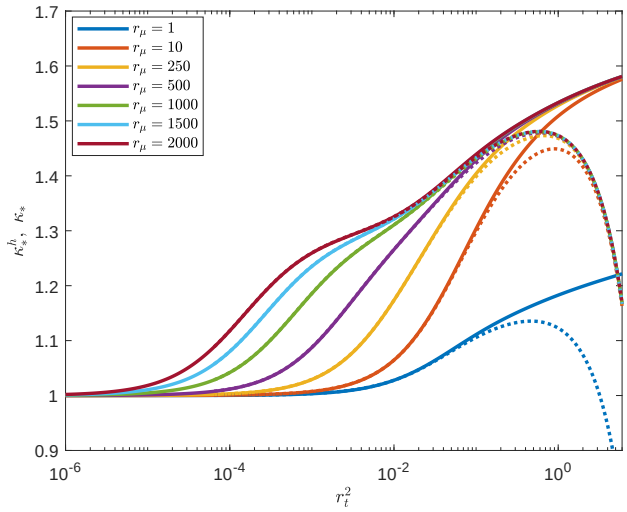

FIG. 8. A comparison between κ_*(dotted line) e κ_*^h (continuous line) as functions of r_t^2, when $R_0 = 1\ \mu$m and different values of r_μ are taken into account.

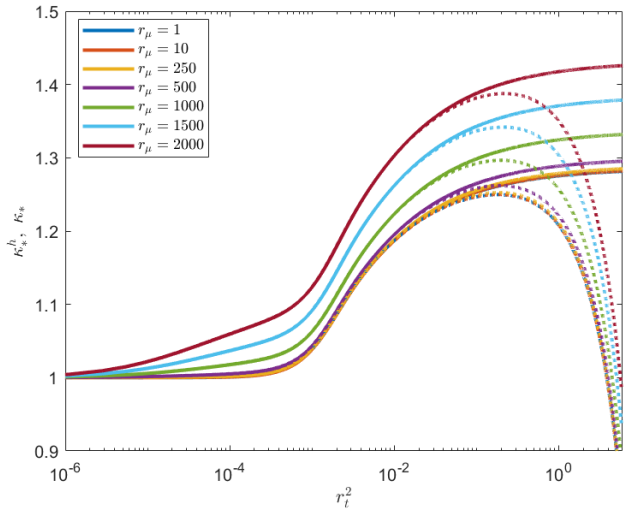

FIG. 9. A comparison between κ_*(dotted line) e κ_*^h (continuous line) as functions of r_t^2, when $\omega = 10^6$ Hz and different values of r_μ are taken into account.

tion of r_t^2 for CO_2 gas (9), varying the oscillation period for fixed R_0 (Fig. 6, 7, 8) or the equilibrium radius for a prescribed acoustic angular frequency (Fig. 9, 10, 11). A comparison between κ_* (dotted line) and κ_*^h (continuous line) is also proposed. When $r_t^2 > 1$, that is to say when the homobaric hypothesis fails, the behaviour of κ_* suddenly changes, decreasing rapidly, in contrast to the polytropic index associated with the homobaric model, which continues to grow tending to its asymptotic value. In each figure the effect of the bulk viscosity (or equivalently of τ_Π) is analysed: it turns out that differences in the generalized polytropic index for different values of μ_b grow when the oscillation frequencies increase, becoming significantly relevant. We also stress that a comparison is possible with what was obtained by Prosperetti[23, 24] for the NSF model, omitting the contribution of the dynamic pressure. In the figures the polytropic indexes obtained in [23, 24] coincide qualitatively with the behaviour of κ_* or κ_*^h corresponding to the lowest value of r_μ. Finally, we remark that if the heat flux equation $(32)_2$ is replaced by the Fourier relation the same results are obtained, at least at the plot precision.

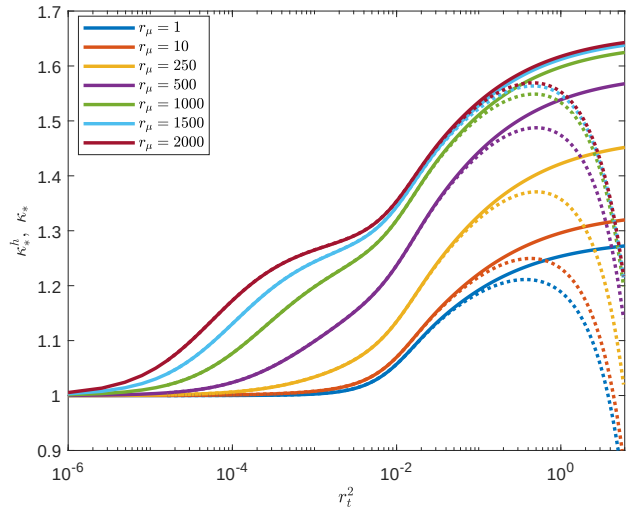

FIG. 10. A comparison between κ_*(dotted line) e κ_*^h (continuous line) as functions of r_t^2, when $\omega = 10^7$ Hz and different values of r_μ are taken into account.

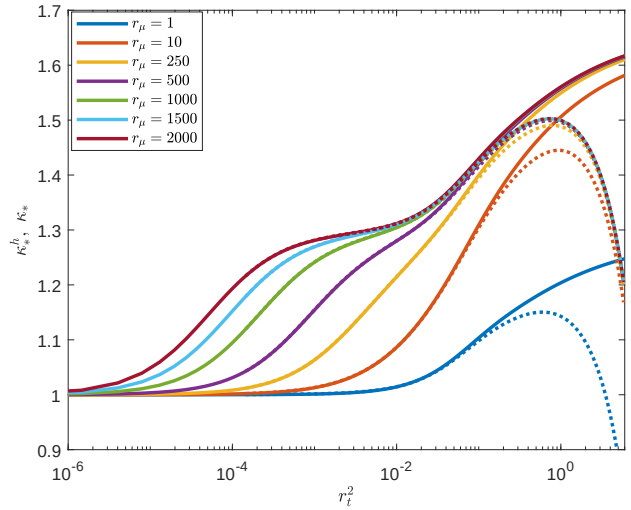

FIG. 11. A comparison between κ_*(dotted line) e κ_*^h (continuous line) as functions of r_t^2, when $\omega = 10^8$ Hz and different values of r_μ are taken into account.

B. Dimensionless homobaric equations

The previous model can be rewritten using the dimensionless variables introduced in (10). After making the behaviour of the relaxation times, which we will express as $\tau_q = \tilde{\tau}_q p/p_g^E$ and $\tau_\Pi = \tilde{\tau}_\Pi p/p_g^E$, more realistic, the homobaric equations are simplified as

$$
\begin{aligned}
&\hat{p}' = \frac{6}{D\hat{R}}\left[-\left(\frac{(D+2)}{2}\hat{p}+\hat{\Pi}\right)\hat{R}' - \hat{q}_R\right],\\
&\hat{\Pi}' = -\frac{2(D-3)\hat{p}+(5D-6)\hat{\Pi}}{D\hat{R}}\hat{R}' - \frac{4(D-3)}{D(D+2)\hat{R}}\hat{q}_R - \frac{\hat{\Pi}\hat{p}}{\bar{\tau}_\Pi},\\
&\left[\frac{(D+2)\hat{p}+2\hat{\Pi}}{2\hat{T}}\right]\left(\partial_{\hat{t}}\hat{T} + \frac{\hat{v}-x\hat{R}'}{\hat{R}}\partial_x\hat{T}\right) -\\
&-\left(1+\frac{\hat{\Pi}}{\hat{p}}\right)\hat{p}' + \frac{1}{\hat{R}}\partial_x\hat{q} = -\frac{2\hat{q}}{\hat{R}x},\\
&\partial_{\hat{t}}\hat{q} + r_t^{-2}\frac{(D+2)\hat{p}+(D+4)\hat{\Pi}}{2\hat{R}}\partial_x\hat{T} = -\frac{\hat{q}\hat{p}}{\bar{\tau}_q} - \frac{2(2D+9)\hat{q}\hat{R}'}{(D+2)\hat{R}},\\
&\hat{v} - \hat{R}'x = -2\frac{\hat{q}-\hat{q}_R x}{(D+2)\hat{p}+2\hat{\Pi}},
\end{aligned}
\tag{39}
$$

where the following notation is introduced: $\hat{p}' = d\hat{p}/d\hat{t}$, $\hat{\Pi}' = d\hat{\Pi}/d\hat{t}$, $\hat{R}' = d\hat{R}/d\hat{t}$, $\bar{\tau}_q = \omega\tilde{\tau}_q$, $\bar{\tau}_\Pi = \omega\tilde{\tau}_\Pi$. We stress that the last equation contains the quantity $r_t^{-2} \gg 1$. Hence, in many approximations we will reduce the heat flux equation to Fourier's, neglecting the remaining terms.

It is usefull to rewrite the approximated Keller Miksis equation (2) in dimensionless form:

$$
\begin{aligned}
&\left(1-\frac{\hat{R}'}{\hat{c}_L}+\frac{4\hat{\mu}_L r_t^{-2}}{\hat{\rho}_L\hat{c}_L\hat{R}}\right)\hat{R}\hat{R}'' + \frac{3}{2}\left(1-\frac{\hat{R}'}{3\hat{c}_L}-\frac{8\hat{\mu}_L r_t^{-2}}{3\hat{\rho}_L\hat{c}_L\hat{R}}\right)\hat{R}'^2 =\\
&= \left(1+\frac{\hat{R}'}{\hat{c}_L}\right)\frac{r_t^{-2}}{\hat{\rho}_L}\hat{p}_l + \frac{r_t^{-2}\hat{R}}{\hat{\rho}_L\hat{c}_L}\left(\hat{p}_g' - \hat{p}_a' + \frac{2\hat{\sigma}_L\hat{R}'}{\hat{R}^2}\right),
\end{aligned}
\tag{40}
$$

where

$$
\hat{p}_l = \frac{p_l}{P_g^E},\ \hat{p}_a = \frac{p_a}{P_g^E},\ \hat{\rho}_L = \frac{\rho_L}{\rho_0},\ \hat{\sigma}_L = \frac{\sigma_L}{P_g^E R_0},\ \hat{\mu}_L = \frac{\mu_L\omega}{P_g^E};
\tag{41}
$$

while, referring to the same dimensionless quantities, the Rayleigh Plesset equation (1) becomes (if $\hat{p}_0 = p_0/P_g^E$)

$$
\hat{R}\hat{R}'' + \frac{3}{2}\hat{R}'^2 = \frac{r_t^{-2}}{\hat{\rho}_L}\left[\hat{p}_g - \hat{p}_0 - \hat{p}_a - \frac{2\hat{\sigma}_L}{\hat{R}} - \frac{4\hat{\mu}_L\hat{R}'}{\hat{R}}\right].
\tag{42}
$$

C. Isothermal regime

The isothermal regime is characterized by the hypothesis that $r_t^{-2}\bar{\tau}_q = \varepsilon^{-1} \gg 1$. Under this condition, two extreme cases can occur for which it is simple to approximate equations (39): in *case 1* $\bar{\tau}_\Pi = \varepsilon \ll 1$ (this case is very close to what is already known in the literature), while in *case 2* $\bar{\tau}_\Pi \simeq \varepsilon^{-1} \gg 1$. Let us therefore introduce a Taylor series expansion of the field variables in the parameter ε

$$
\begin{aligned}
&\hat{p} = \hat{p}_{(0)} + \varepsilon\hat{p}_{(1)} + O(\varepsilon^2), \quad \hat{\Pi} = \hat{\Pi}_{(0)} + \varepsilon\hat{\Pi}_{(1)} + O(\varepsilon^2),\\
&\hat{T} = \hat{p}_{(0)} + \varepsilon\hat{T}_{(1)} + O(\varepsilon^2), \quad \hat{q} = \hat{q}_{(0)} + \varepsilon\hat{q}_{(1)} + O(\varepsilon^2),\\
&\hat{v} = \hat{v}_{(0)} + \varepsilon\hat{v}_{(1)} + O(\varepsilon^2).
\end{aligned}
\tag{43}
$$

1. Case 1

In case 1, the approximation of (39) at zeroth order gives the following relations:

$$\begin{aligned} &\hat{T}_{(0)} = 1, \quad \hat{p}_{(0)} = \hat{R}^{-3}, \quad \hat{\Pi}_{(0)} = 0, \\ &\hat{q}_{(0)} = -\hat{R}'\hat{R}^{-3}x, \quad \hat{v}_{(0)} = \hat{R}'x, \end{aligned} \tag{44}$$

in complete agreement with what is known in the literature[24]. At the next order of the Taylor expansion, however, differences can observed due to the presence of the dynamic pressure:

$$\begin{aligned} &\hat{T}_{(1)} = \frac{\hat{R}'}{(D+2)\hat{R}^2}(x^2-1), \quad \hat{p}_{(1)} = -\frac{2\hat{R}'}{5(D+2)\hat{R}^5}, \\ &\hat{\Pi}_{(1)} = -\frac{2(D-3)}{(D+2)}\frac{\hat{R}'}{\hat{R}}, \quad \hat{v}_{(1)} = -\frac{\hat{R}''\hat{R}-2\hat{R}'^2}{10\hat{R}^5}(x^3-x), \\ &\hat{q}_{(1)} = -\frac{x^3(\hat{R}''\hat{R}-2\hat{R}'^2)}{10\hat{R}^5} + \\ &+\frac{x((5D+6)\hat{R}''\hat{R}+10(6(D-3)\hat{R}^4-D)\hat{R}'^2)}{30(D+2)\hat{R}^5}. \end{aligned} \tag{45}$$

2. Case 2

Assuming that the relaxation time of the dynamic pressure is larger than the oscillation period of the bubble, the Taylor series expansion predicts a different behaviour of the total gas pressure already at zeroth order:

$$\begin{aligned} &\hat{T}_{(0)} = 1, \quad \hat{p}_{(0)} = \hat{R}^{-3}, \quad \hat{\Pi}_{(0)} = \hat{R}^{-\frac{5D}{D+2}} - \hat{R}^{-3}, \\ &\hat{q}_{(0)} = -\hat{R}'\hat{R}^{-\frac{5D}{D+2}}x, \quad \hat{v}_{(0)} = \hat{R}'x. \end{aligned} \tag{46}$$

Hence, the total pressure of the gas, even for a constant temperature inside the bubble, is supposed to depend on the parameter D, and more precisely, on the ratio of the specific heats: $p_{(0)} + \Pi_{(0)} = \hat{R}^{-5/\gamma}$. Consequently, in isothermal regime, if the Rayleigh Plesset or the Keller Miksis equations are used in closed form, different behaviours can be expected depending on the ratio of the specific heats γ and on the small/large value of μ_b. See, for example, Figure 12 that shows the behaviour of R in case 1 and case 2 for different values of D, if $T_0 = 300$ K, CO_2 is the gas (9) and H_2O is the liquid around the bubble (3), $P_{a0} = 10^5$ Pa and the angular frequency of the acoustic pressure is $\omega = 10^6$ Hz. The results are obtained referring to the approximated Keller Miksis equation and inserting the sum of equilibrium and dynamic pressure at zeroth order ($p_g = p_{(0)} + \Pi_{(0)}$) as total gas pressure. There is therefore no doubt that bulk viscosity can have observable effects on the dynamics of the bubble if the equilibrium radius of the bubble is sufficiently small and the oscillation angular frequency sufficiently large. Referring to Fourier relation, in

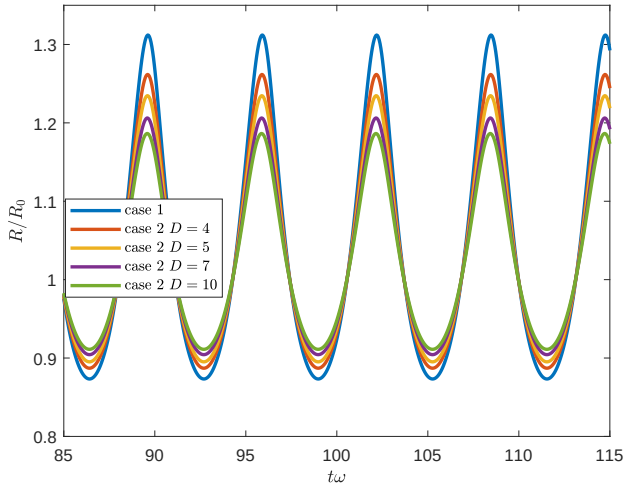

FIG. 12. The bubble's radius in the isothermal regime in case 1 and case 2 for different values of D when $R_0 = 1\mu$m, $P_{a0} = 10^5$ Pa, $\omega = 10^6$ Hz.

case 2 the first-order Taylor expansion gives

$$\begin{aligned} &\hat{T}_{(1)} = \frac{\hat{R}'(x^2-1)}{2\hat{R}^{\frac{5D}{D+2}}}, \quad \hat{p}_{(1)} = -\frac{\hat{R}'}{5\hat{R}^{\frac{2(4D+3)}{D+2}}}, \\ &\hat{\Pi}'_{(1)} = -\frac{5D\hat{\Pi}_{(1)}\hat{R}'}{(D+2)\hat{R}} + \frac{4(4D^2-9D-9)\hat{R}'^2}{15(D+2)^2\hat{R}^{\frac{9D+8}{D+2}}} - \\ &-\frac{2(D-3)\hat{R}''}{15(D+2)\hat{R}^{\frac{8D+6}{D+2}}} - \frac{\hat{\Pi}_{(0)}}{\hat{R}^3} \\ &\hat{q}_{R(1)} = -\hat{\Pi}_{(1)}\hat{R}' + \frac{(12+6D-5D^2)\hat{R}'^2}{30(D+2)\hat{R}^{\frac{8D+6}{D+2}}} + \frac{D\hat{R}''}{30\hat{R}^{\frac{7D+4}{D+2}}}, \end{aligned} \tag{47}$$

where for the sake of simplicity we have omitted the cumbersome explicit expression of $\hat{q}_{(1)}$.

D. Adiabatic regime

The adiabatic regime is characterized by the condition $\hat{\tau}_q r_t^{-2} = \varepsilon \ll 1$, so that it is reasonable to neglect the heat flux in equations (39). This condition is typical of gas bubbles with a large radius or when the bubble's shrinkage happens very quickly[8, 9]. In this framework two extreme cases will be analyzed: in *case 3* $\hat{\tau}_\Pi = \varepsilon$ (in this way the dynamic pressure is also negligible and results close to those known in the literature are obtained), while in *case 4* $\hat{\tau}_\Pi = 1/\varepsilon$ (a condition difficult to observe in the asymptotic behavior of the solutions, since extremely high bulk viscosities would be required in the range of validity of homobaricity). Before moving on to the results obtained in these two cases, it is important to underline that the adiabatic regime is thermodynamically unrealistic in the presence of dissipation. It is, in fact, easy to verify that balance laws containing dissipative terms in the absence of heat flux, coupled with the Rayleigh Plesset or the Keller Miksis

equation would predict relevant asymptotic drift phenomena of the oscillation radius, not compatible with the experimental data[8, 9]. This effect occurs for example if we refer to the RET model with 6 moments $ET_{6,P}$ in which the only dissipative term is associated with the dynamic pressure, while the heat flux is assumed to be negligible. On the other hand, it has already been proven that the Euler model for a gas predicts temperatures which in some regimes are not compatible with experiments[26]. The previous considerations place the adiabatic approximation as a simple, but incomplete and imprecise tool for describing the thermodynamics of bubble oscillation.

1. Case 3

Introducing the Taylor's expansion (43), in equations (39), it is easily verified that the zeroth order is in complete agreement with the results commonly presented in the literature[2, 4, 7, 9, 21, 23]:

$$\begin{aligned} &\hat{q}_{(0)} = 0, \quad \hat{\Pi}_{(0)} = 0, \quad \hat{p}_{(0)} = \frac{1}{\hat{R}^{\frac{3(D+2)}{D}}}, \\ &\hat{T}_{(0)} = \frac{1}{\hat{R}^{\frac{6}{D}}}, \quad \hat{v}_{(0)} = \hat{R}' x. \end{aligned} \tag{48}$$

In this framework the solution turns out to be incompatible with the boundary condition $T|_R = T_0$ in $r = R$. In fact, in the case of a large bubble it is usually assumed that the gas behaves adiabatically, but there is a layer around the interface between liquid and gas in which heat exchange is observed[24]. The contribution of the dynamic pressure is present instead at the first order:

$$\Pi_{(1)} = -\frac{2(D-3)\hat{R}'}{D\hat{R}}. \tag{49}$$

2. Case 4

In this last case the contribution of μ_b produces effects already at the zeroth order of the Taylor expansion. Such effects, as we have already mentioned, are often incompatible with the homobaric hypothesis. It must be said, however, that they could be realistic over short times: during the initial transient time or in the final part of the bubble shrinkage in a regime close to sonoluminescence. Imposing that the bubble is initially ($\hat{t} = 0$) at equilibrium, it implies that $\hat{\Pi}(0) = 0$ when $\hat{R}(0) = 1$. Thus, the approximation (43) in (39) gives the following zeroth order terms:

$$\begin{aligned} &\hat{q}_{(0)} = 0, \quad \hat{v}_{(0)} = \hat{R}' x, \quad \hat{p}_{(0)} = \frac{3}{D\hat{R}^5} + \frac{D-3}{D\hat{R}^3}, \\ &\hat{\Pi}_{(0)} = \frac{D-3}{D}\left(\frac{1}{\hat{R}^5} - \frac{1}{\hat{R}^3}\right), \quad \hat{T}_{(0)} = 1 + \frac{3}{D}\left(\frac{1}{\hat{R}^2} - 1\right). \end{aligned} \tag{50}$$

It is evident that the total gas pressure at zeroth order does not depend on the number of molecular degrees of freedom, but its expression coincides with the adiabatic behaviour of a monatomic gas. This fact is in complete agreement with the asymptotic behaviour of κ^h_* for high values of bulk viscosity. This, however, goes beyond the range of validity of the homobaric hypothesis, if small amplitude oscillations are taken into account. Nevertheless, in many studies the value of the polytropic index is chosen equal to γ, ignoring the issue related to homobaricity. Also for this reason, the possible role that dynamic pressure and bulk viscosity might play in a simulation of the bubble dynamics is of great relevance. Finally, through Laplace transforms and Tauberian theorems [24] it is verified that during an initial time interval the behaviour of the gas could always be expressed as adiabatic. Therefore, Π is relevant even in the initial phases of the bubble's oscillations. In Figure 13 the behaviour of the radius R in the adiabatic regime is compared under the conditions of cases 3 and 4 in the zeroth order Taylor expansion ($p_g = p_{(0)} + \Pi_{(0)}$). Here we refer to the approximated Keller Miksis equation, prescribing the physical parameters as $T_0 = 300$ K, $P_{a0} = 4 \times 10^4$ Pa, $\omega = 10^4$ Hz, $R_0 = 100$ μm, (3) and (9). Note how the γ dependence is observable only for small values of $\bar{\tau}_\Pi$, when the role of the dynamic pressure can be neglected. Moreover, in the limit of a polyatomic gas tending to a monatomic one the results of case 3 and case 4 coincide ($D \to 3$).

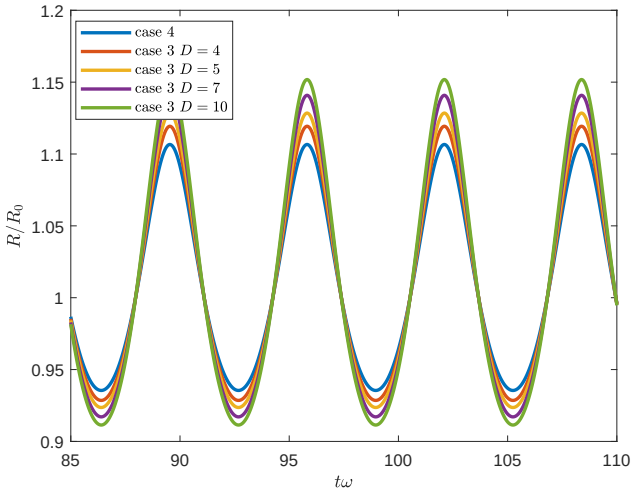

FIG. 13. The bubble's radius in the adiabatic regime in case 3 and case 4 for different values of D when $R_0 = 100$ μm, $P_{a0} = 4 \times 10^4$ Pa, $\omega = 10^4$ Hz.

VII. FURTHER SIMPLIFICATION OF THE HOMOBARIC MODEL AND NUMERICAL INTEGRATION

The numerical integration of equations (30), (31) and (32), coupled to the ODE that rules the radius dynamics, could be a hard task over long periods of time, in particular due to the presence of two hyperbolic balance laws (32) equipped with dissipative terms and time-dependent coefficients. On the other hand, an analysis over time scales much larger than the single oscillation period is often required. Inspired by the

results obtained in the case of isothermal regimes and by the technique proposed by Zhou and Prosperetti [10], we introduce at this point a further simplification of the homobaric model by imposing that the behaviour of temperature and heat flux is polynomial, in order to reduce the numerical approach to the integration of a set of ODEs. Therefore, let us assume that

$$\hat{T} = A_1 + A_2 x^2 + A_3 x^4, \qquad \hat{q} = A_4 x + A_5 x^3. \tag{51}$$

Since the field variables are defined in a bounded interval ($x \in [0,1]$), boundary conditions must be imposed: $q(x=0)=0$ (already in agreement with (51)) and $T(x=1)=T_0$, that is to say $\hat{T}(x=1)=1$ (that implies $A_3 = 1-A_1-A_2$).

Taking into account the approximations made and the impossibility of describing in detail the dynamics of the gas inside the bubble after the simplifications, it is reasonable to focus on the average behaviour of temperature and heat flux (coherently with the procedure introduced in [10] for a model deduced from the NSF equations) and construct suitable equations for the temperature and heat flux averages calculated on the dimensionless volume of the bubble. For this purpose, the averaged values are defined as

$$\langle \hat{T} \rangle = 3\int_0^1 x^2 \hat{T}(x)dx, \quad \langle \hat{q} \rangle = 3\int_0^1 x^2 \hat{q}(x)dx, \tag{52}$$

and equations $(39)_{3,4}$ become

$$\begin{aligned}
&\partial_t \langle \hat{T} \rangle + \frac{6\hat{R}'(\hat{p}+\hat{\Pi})\langle \hat{T} \rangle}{D\hat{p}\hat{R}} + \frac{12(\hat{p}+\hat{\Pi})\hat{q}_R\langle \hat{T} \rangle}{D\hat{p}((D+2)\hat{p}+2\hat{\Pi})\hat{R}} + \\
&+ \frac{2\langle \hat{T}\partial_x \hat{q} \rangle + 4\langle \hat{q}\hat{T}x^{-1} \rangle - 2\langle (\hat{q}-\hat{q}_R x)\partial_x \hat{T} \rangle}{(D+2)\hat{p}+2\hat{\Pi})\hat{R}} = 0, \\
&\partial_t \langle q \rangle + r_t^{-2}\frac{(D+2)\hat{p}+(D+4)\hat{\Pi}}{2\hat{R}}\langle \partial_x \hat{T} \rangle = \\
&= -\frac{\langle \hat{q} \rangle \hat{p}}{\bar{\tau}_q} - 2\frac{(2D+9)\langle \hat{q} \rangle \hat{R}'}{(D+2)\hat{R}}.
\end{aligned} \tag{53}$$

Furthermore, the values of the temperature at the centre of the bubble ($\hat{T}_c = \hat{T}(x=0) = A_1$) and of the heat flux in the liquid/gas interface $\hat{q}_R = \hat{q}(x=1) = A_4 + A_5$ should satisfy dimensionless equations deduced from (39):

$$\begin{aligned}
&\hat{T}_c' = -6\hat{T}_c\left[\frac{(\hat{p}+\hat{\Pi})\hat{R}' + A_4}{D\hat{p}\hat{R}} + \frac{2A_5(\hat{p}+\hat{\Pi})}{D\hat{p}[(D+2)\hat{p}+2\hat{\Pi}]\hat{R}}\right], \\
&\hat{q}_R' = -r_t^{-2}(2A_2+4A_3)\frac{(D+2)\hat{p}+(D+4)\hat{\Pi}}{2\hat{R}} - \\
&- \frac{\hat{q}_R\hat{p}}{\bar{\tau}_q} - \frac{2(2D+9)\hat{R}'\hat{q}_R}{(D+2)\hat{R}}.
\end{aligned} \tag{54}$$

With simple algebraic steps it is possible to obtain the simplified system of ODEs for A_1, A_2, A_4, A_5,

$$\begin{aligned}
A_1' &= -\frac{6A_1A_4 + 6\hat{R}'A_1(\hat{p}+\hat{\Pi})}{D\hat{p}\hat{R}} - \frac{12A_1A_5(\hat{p}+\hat{\Pi})}{D\hat{p}((D+2)\hat{p}+2\hat{\Pi})\hat{R}}, \\
A_2' &= -\frac{3(2A_2+5)A_4}{D\hat{p}\hat{R}} - \frac{2A_2A_5((23D+54)\hat{p}+54\hat{\Pi})}{9D\hat{p}((D+2)\hat{p}+2\hat{\Pi})\hat{R}} - \\
&- \frac{3(2A_2+5)\hat{R}'(\hat{p}+\hat{\Pi})}{D\hat{p}\hat{R}} - \frac{5A_5((54+(43+20A_1)D)\hat{p}+54\hat{\Pi})}{9D\hat{p}((D+2)\hat{p}+2\hat{\Pi})\hat{R}}, \\
A_4' &= -\frac{A_4\hat{p}}{\bar{\tau}_q} - \frac{2A_4(2D+9)\hat{R}'}{(D+2)\hat{R}} - \frac{A_2 r_t^{-2}((D+2)\hat{p}+(D+4)\hat{\Pi})}{\hat{R}}, \\
A_5' &= -\frac{A_5\hat{p}}{\bar{\tau}_q} - \frac{2A_5(2D+9)\hat{R}'}{(D+2)\hat{R}} - \\
&- \frac{2(1-A_1-A_2)r_t^{-2}((D+2)\hat{p}+(D+4)\hat{\Pi})}{\hat{R}}.
\end{aligned} \tag{55}$$

In what follows, the numerical integration of the system of ordinary differential equations has been performed with ©Matlab.

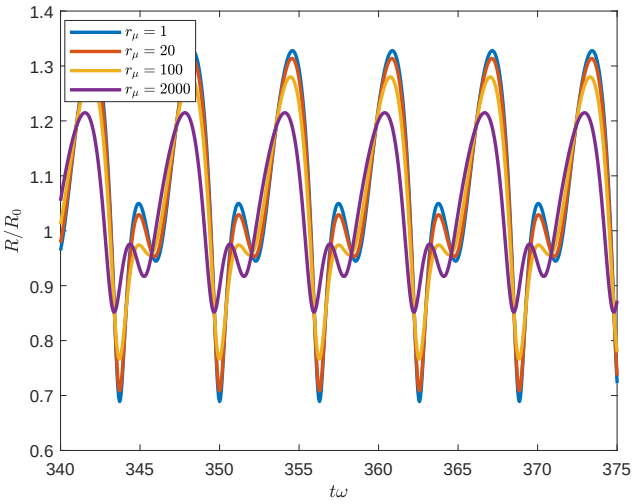

FIG. 14. The $R(t)$ oscillations after the transient time if $R_0 = 1\ \mu$m, $P_{a0} = 8\times10^4$ Pa and $\omega = 1.24\times10^7$ Hz. Different values of r_μ are considered in the case of CO_2 gas.

A. Long time behaviour

The approximate model that we built in the previous sections has the advantage of being easily integrated over a large number of oscillation periods. This aspect is important when a study of the bubble behaviour beyond the transient time is required. It should also be remarked that the presence of a strong dissipation could reduce this transient. Here we present some examples of numerical integration of $(39)_{1,2}$ and (55) coupled with the dimensionless Rayleigh-Plesset equation (42). In particular, Figures 14-22 show the steady state oscillations

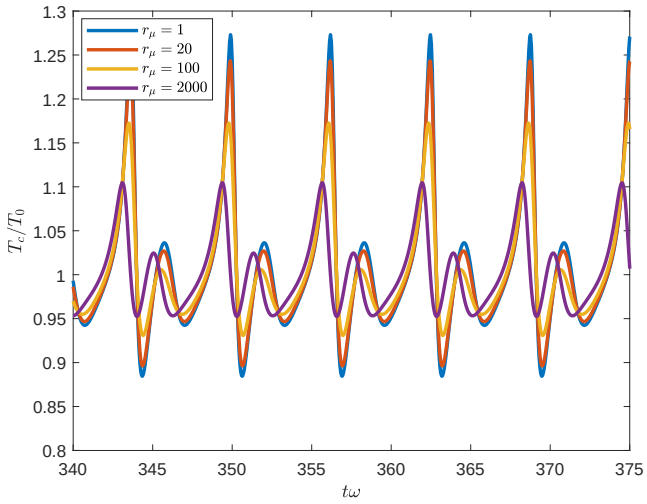

FIG. 15. The T_c oscillations after the transient time under the same assumptions of Fig. 14.

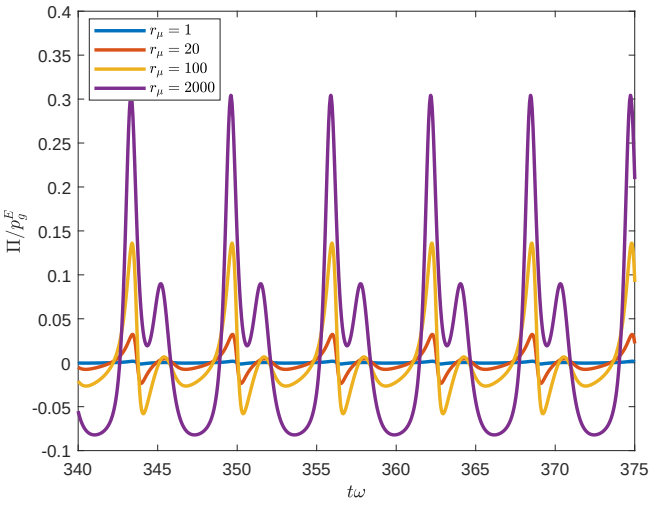

FIG. 16. The Π oscillations after the transient time under the same assumptions of Fig. 14.

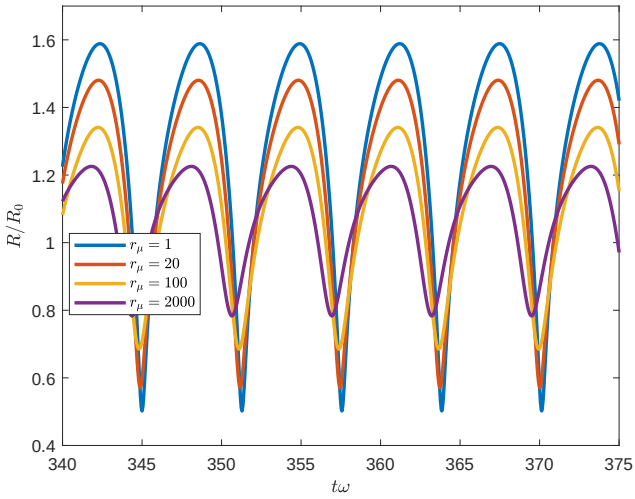

FIG. 17. The $R(t)$ oscillations after the transient time if R_0 and P_{a0} are the same as in Fig. 14, while $\omega = 2.12 \times 10^7$ Hz. Different values of r_μ are considered in the case of CO_2 gas.

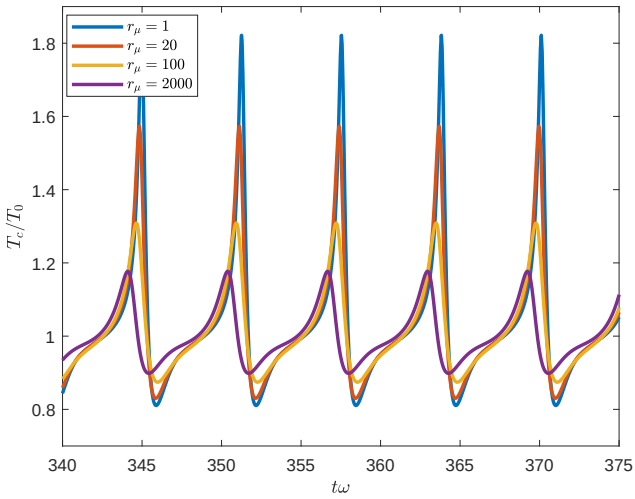

FIG. 18. The T_c oscillations after the transient time under the same assumptions of Fig. 17.

of radius R, temperature T_c and dynamic pressure Π at the centre of the bubble, as r_μ varies and different initial physical conditions or different acoustic pressure are prescribed. A CO_2 gas, (9), bubble immersed in water, (3), is always taken into consideration. In Figures 14-16 R, T_c and Π are presented when $R_0 = 1$ μm, $P_{a0} = 8 \times 10^4$ Pa, $\omega = 1.24 \times 10^7$ Hz, while Figures 17, 18 and 19 show the oscillation of all the quantities when $\omega = 2.12 \times 10^7$ Hz (a value close to the resonance one), for the same initial bubble and the same pressure amplitude as the previous case. Moving on to the case of an equilibrium radius of 10 μm (with $P_{a0} = 5 \times 10^4$ Pa, $\omega = 9.23 \times 10^5$ Hz), it is clear from Figures 20, 21 and 22 that the dissipation effect becomes less incisive unless we are in the presence of very high bulk viscosity values. This observation is consistent with the idea that in a larger bubble oscillating at a lower frequency the dynamic pressure has time to relax before the oscillation is complete.

Under homobaric conditions, as the radius of the bubble increases the differences between the behaviours of the solutions for different values of r_μ become gradually less accentuated until they are completely negligible. Simultaneously, the thermodynamic regime of the bubble moves away from the isothermal conditions typical of very small bubbles. The phase differences in the oscillations that are observed as r_μ varies are a well-known effect of damping in a forced oscillator.

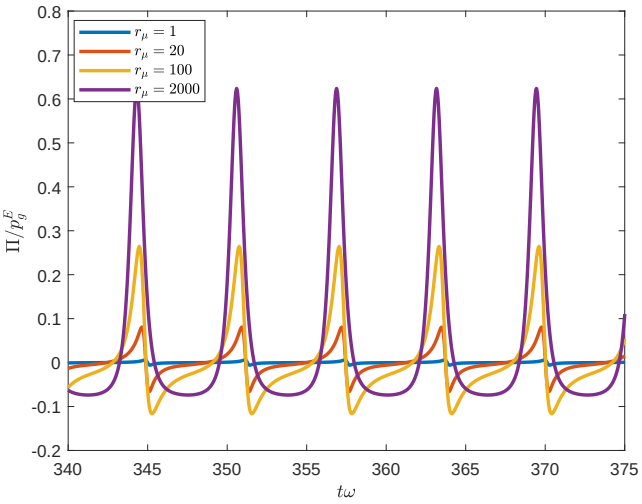

FIG. 19. The Π oscillations after the transient time under the same assumptions of Fig. 17.

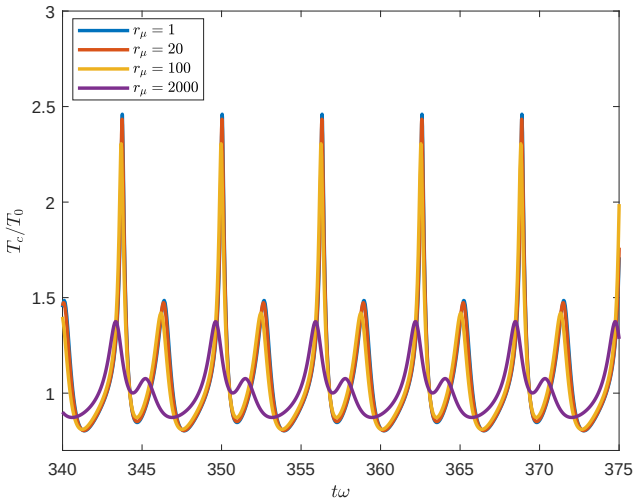

FIG. 21. The T_c oscillations after the transient time under the same assumptions of Fig. 20.

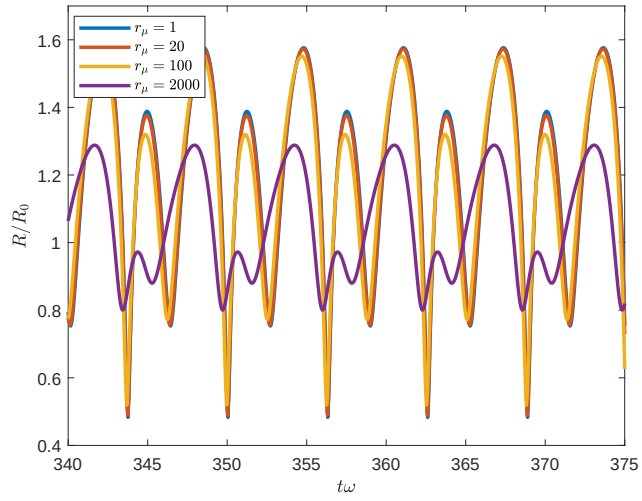

FIG. 20. The $R(t)$ oscillations after the transient time if $R_0 = 10\ \mu$m, $P_{a0} = 5 \times 10^4$ Pa, $\omega = 9.23 \times 10^5$ Hz. Different values of r_μ are considered in the case of CO_2 gas.

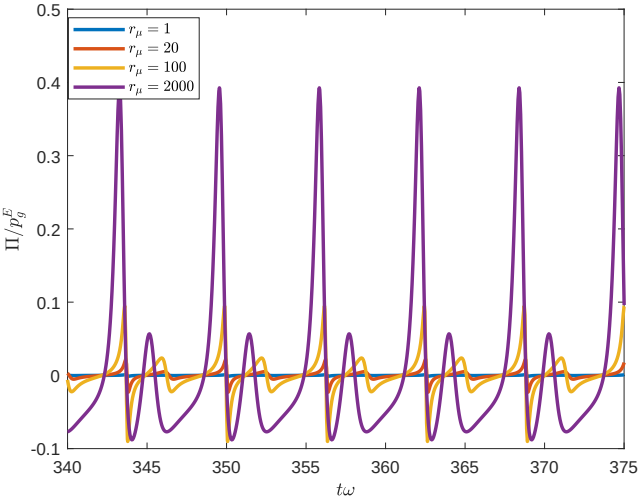

FIG. 22. The Π oscillations after the transient time under the same assumptions of Fig. 20.

B. The dynamic pressure behaviour

In the previous Figures 16, 19 and 22 we have already shown the behaviour of the dynamic pressure in some examples of steady state oscillations for a moderate amplitude of the acoustic signal. Here, we present some further examples with the aim of comparing the trends of dynamic pressure and bubble radius oscillations. The equations for the gas are coupled with the Rayleigh-Plesset equation and integrated following the procedure described in this section. In all cases we consider two very different time intervals: the first transient time (first row of pictures) and the case of the steady state oscillations (second row of pictures). To explore the action of dynamic pressure and bulk viscosity and to determine if it is significantly modified by the dimensions of the bubble at equilibrium, we analyse three different situations: in Figure 23 $R_0 = 1\ \mu$m (we are therefore in the presence of a very small bubble), an intermediate value equal to $R_0 = 10\ \mu$m is taken into account in Figure 24, while the case $R_0 = 100\ \mu$m is shown in Figure 25. In all figures three values of r_μ are compared: 2, 200 e 2000 (first, second and third column of pictures respectively). The highest values of the dynamic pressure are observable in correspondence with sudden variations in the bubble radius: these variations are characteristic of the shrinkage phases. Furthermore, the presence of bulk viscosity can significantly reduce the duration of the initial transient and visibly modify the steady state oscillation of R. As

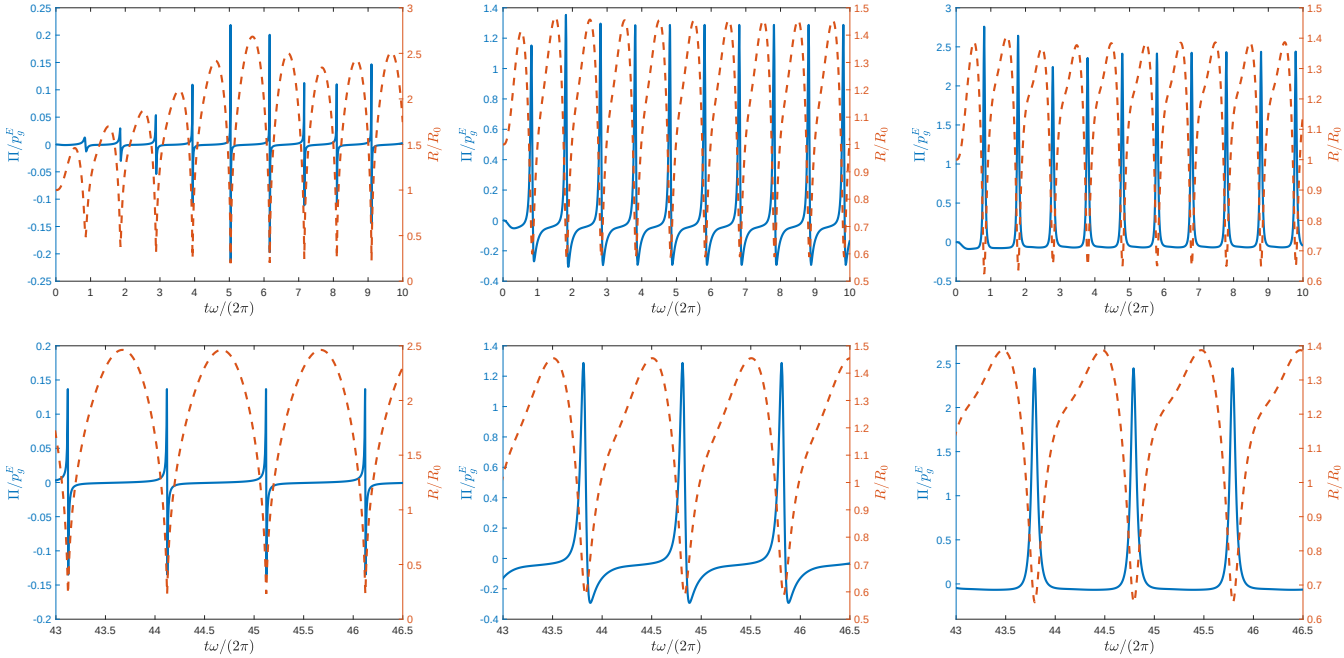

FIG. 23. The Π (continuous line) and the R (dashed line) oscillations as functions of the number of cycles when $R_0 = 1\ \mu$m, $P_{a0} = 1.4 \times 10^5$ Pa, $\omega = 1.89 \times 10^7$ Hz. The first column of pictures presents the case of $r_\mu = 2$, in the second column $r_\mu = 200$, while in the last column $r_\mu = 2000$. In the first row of figures the behaviour at the initial transient time is shown, while in the second row the steady state oscillations are presented.

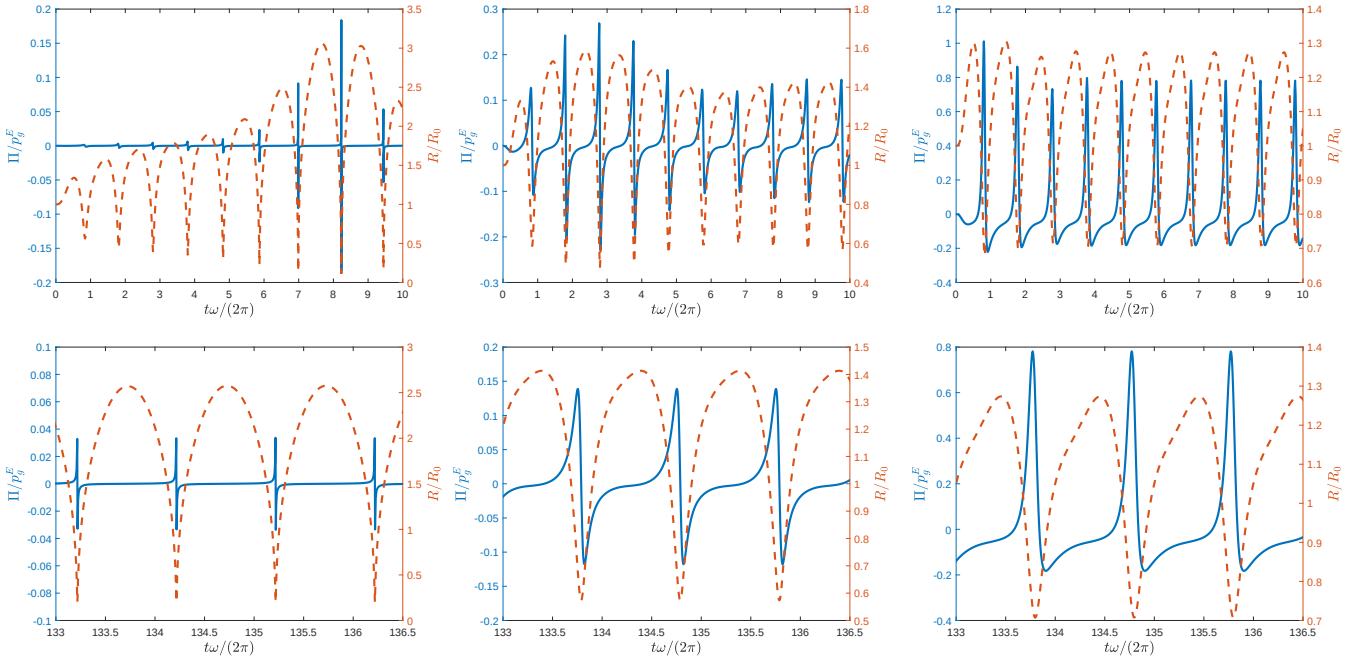

FIG. 24. The Π (continuous line) and the R (dashed line) oscillations as functions of the number of cycles when $R_0 = 10\ \mu$m, $P_{a0} = 6 \times 10^4$ Pa, $\omega = 1.46 \times 10^6$ Hz. The first column of pictures presents the case of $r_\mu = 2$, in the second column $r_\mu = 200$, while in the last column $r_\mu = 2000$. In the first row of figures the behaviour at the initial transient time is shown, while in the second row the steady state oscillations are presented.

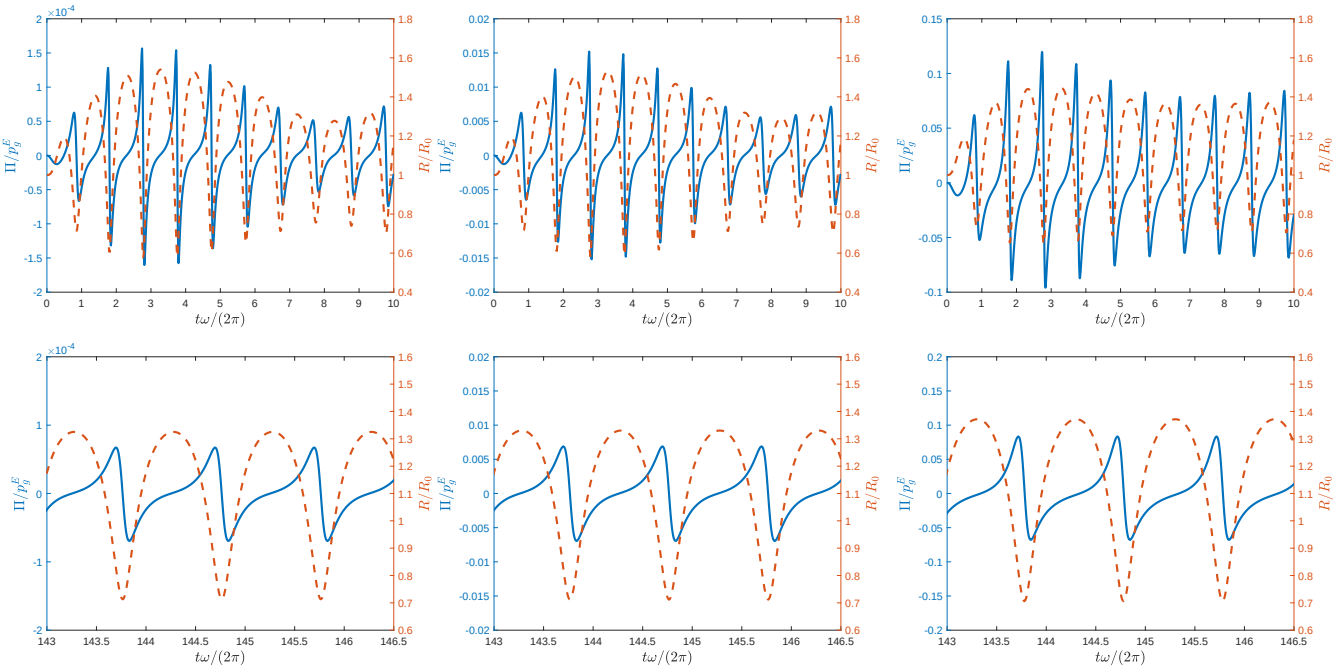

FIG. 25. The Π (continuous line) and the R (dashed line) oscillations as functions of the number of cycles when $R_0 = 100\ \mu$m, $P_{a0} = 3.7 \times 10^4$ Pa, $\omega = 1.53 \times 10^5$ Hz. The first column of pictures presents the case of $r_\mu = 2$, in the second column $r_\mu = 200$, while in the last column $r_\mu = 2000$. In the first row of figures the behaviour at the initial transient time is shown, while in the second row the steady state oscillations are presented.

is known, in damped and forced oscillators relaxation terms can also produce remarkable phase shifts, easily detectable in Figures 23-25. As the equilibrium radius increases, the action of the bulk viscosity becomes less and less incisive, unless extremely high - and therefore unphysical- values of r_μ are prescribed.

C. Frequency response curves

Since the behaviour of the bubble radius is described by the equation of a non-linear oscillator, it is natural to use common oscillator study tools to better understand the characteristics of the phenomenon and to quickly compare the effects that different models of gas dynamics can predict. Among these instruments, a special place in the literature is occupied by the frequency response curve, which Lauterborn made the first use of in the field of cavitation and oscillating bubbles [21]. From these studies it was possible to observe the presence of hysteresis phenomena in correspondence with harmonic, subharmonic and ultraharmonic resonances. Such phenomena can be observed experimentally through an acoustic detector. In particular, the presence of a resonance at a frequency equal to half the harmonic resonance frequency appears to be one of the characteristics used to reveal the presence of bubbles in the liquid.

Here we will consider frequency response curves with the purpose of comparing the homobaric model derived from RET for different values of r_μ, in order to show how a high bulk viscosity can give rise to significant differences both in the values of the resonance frequencies and in the intensity of the oscillation. Like several authors in the literature, we will refer to the simple Rayleigh Plesset model (1) [9, 21]. In this regard, let us remind that the natural frequency of the linearized oscillator associated with (1) is easily determined as (Minnaert was the first researcher to introduce this idea[70]) [9]:

$$\nu_n = \frac{1}{2\pi R_0}\sqrt{\frac{3\kappa p_0}{\rho_L} + (3\kappa - 1)\frac{2\sigma_L}{\rho_L R_0}}, \tag{56}$$

while from the theory of the forced and damped harmonic oscillator the resonance frequency of the linearized oscillator turns out to be

$$\nu_{ris} = \frac{1}{2\pi R_0}\sqrt{\frac{3\kappa p_0}{\rho_L} + (3\kappa - 1)\frac{2\sigma_L}{\rho_L R_0} - \frac{8\mu_L^2}{\rho_L^2 R_0^2}}, \tag{57}$$

where κ denotes the polytropic index. In the present work κ should be replaced by the generalized polytropic index κ_* or by its homobaric approximation κ_*^h. A couple of examples of frequency response curves are shown in figures 26 and 27, where the symbol R_{max} corresponds to the maximum value of the bubble radius during its steady state oscillations. The figures are obtained through the numerical integration of (42), $(39)_{1,2}$ and (55).

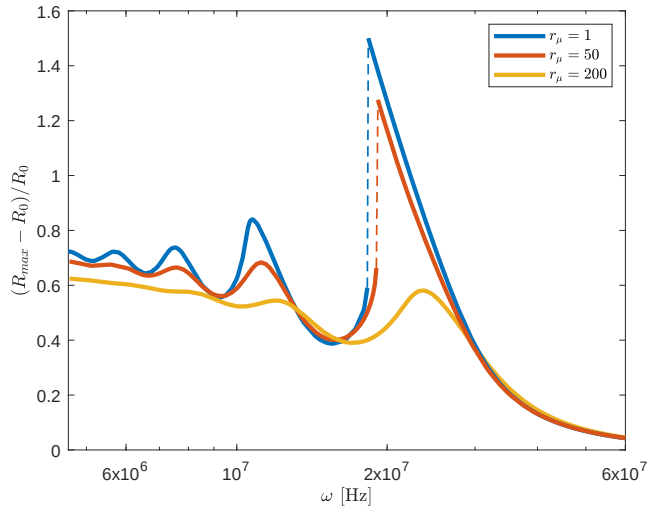

FIG. 26. The frequency response curve for a CO_2 gas bubble in water when $R_0 = 1$ μm and $P_{a0} = 1.3 \times 10^4$ Pa; different values of r_μ are considered.

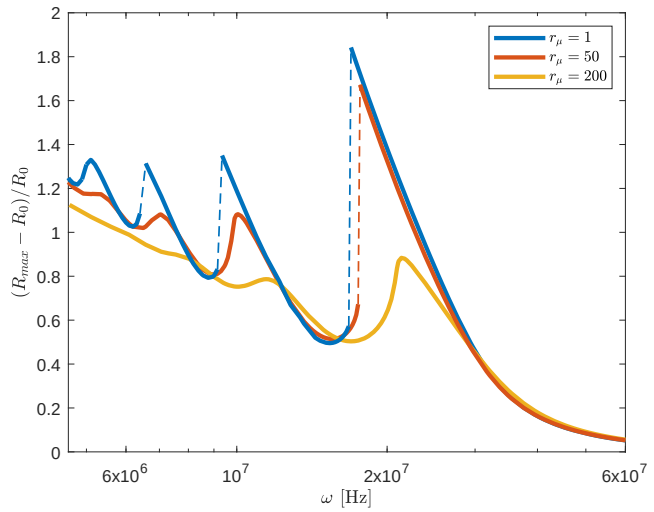

FIG. 27. The frequency response curve for a CO_2 gas bubble in water when $R_0 = 1$ μm and $P_{a0} = 1.6 \times 10^4$ Pa; different values of r_μ are considered.

D. Nearly sonoluminescence regime

Sonoluminescence is a surprising and peculiar effect that occurs during the oscillation of a bubble within a liquid under special conditions of bubble size,and of frequency and amplitude of the acoustic pressure. It has fascinated scientists for decades since it was discovered by chance in 1934 by Frenzel and Schultes[71]. The dynamic regime that is associated with the emission of light is characterized by highly non-linear oscillations in which the bubble expands until it reaches a maximum radius R_M equal to 10 times the equilibrium one. The expansion is followed by a rapid and abrupt contraction in

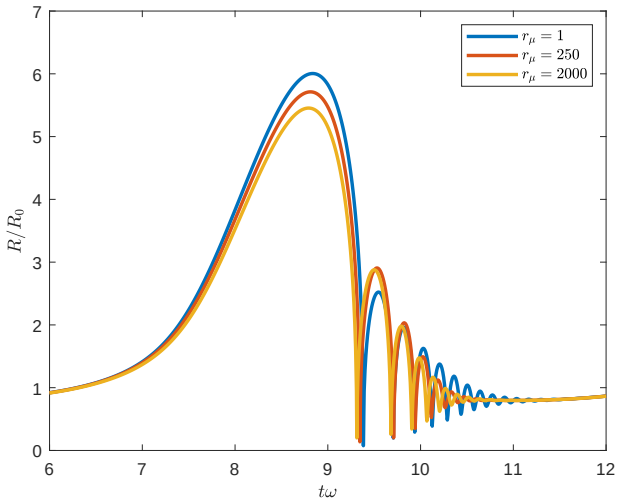

FIG. 28. The $R(t)$ behaviour in a nearly sonoluminescence regime in the case of CO_2 for different values of r_μ.

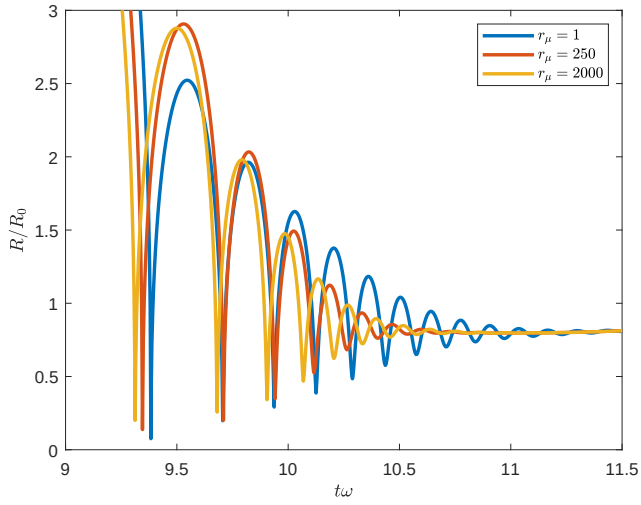

FIG. 29. A zoom on the rebounds of figure 28.

which $R(t)$ goes from values of the order of $10R_0$ to values well below $R_0/2$ [2, 5, 7–9]. In the final stages of this shrinkage, the emission of a flash of light is observed. Rebounds follow which gradually diminish, before the phenomenon repeats itself again. The physical-mathematical description of this phenomenon is very complex and challenging, but for the sake of simplicity also in this framework it is often left to the approximated Keller Miksis or Rayleigh Plesset equation, made self standing by a pressure law as a power of the radius [4, 7, 9].

Wu and Roberts[25] conducted a famous analysis of the problem by coupling the set of conservation laws of an Euler gas to one of these equations. Various models were then introduced to take thermodynamic effects into account and predict temperatures close to those deduced from experiments[4, 5,

7, 8, 26, 48] It should be noted, however, that for a correct and faithful modelling of the SL it would be appropriate to introduce further details such as the dependence of the physical constants (for example heat conductivity and viscosity) on the temperature, the non-ideality and non-polytropicity of the gas, the presence of other gases. Moreover, the homobaricity could decline as well[8, 48].

In this subsection we test the simplified homobaric equations derived in the Section VII only at a qualitative level and under conditions close but not coinciding with those of sonoluminescence. We leave the direct integration of equations (8) to future studies, since the objective of the present analysis is to verify whether the presence of Π could give rise to measurable effects in these extreme scenarios.

Figure 28 shows how relevant a high value of bulk viscosity could be. The results are obtained for a driving pressure amplitude $P_{a0} = 1.2 \times 10^5$ Pa and a driving frequency $\nu = 26.5$ kHz, while the equilibrium radius of the bubble is assumed to be $R_0 = 4.5$ μm. The figure refers to the case of CO_2 gas and H_2O liquid, (3) and (9), and is obtained by integrating numerically the ODE system composed of equations $(39)_{1,2}$ and (55) coupled with the approximated Keller Miksis equation (40). Differences are observable in the R_M value, in the duration of the contraction, and in the rebounds (see the zoom of Fig. 29) which dampen more quickly after the first one. We point out that for small values of r_μ the behaviour of R coincides with that predicted by the homobaric model deduced from NSF equations [10].

VIII. CONCLUSIONS

Those associated with the dynamics of gas bubbles in liquids are highly non-linear and complex phenomena, that involve multiple aspects of mathematics, physics and chemistry. The ever-growing interest in their possible applications has inspired many works over the years, in which researchers attempted to establish what the indispensable ingredients were for the construction of a mathematical model capable of reliable quantitative or at least qualitative predictions. In the past, the possible role of dynamic pressure for gases with high bulk viscosity has never been examined in the framework of cavitation. In the present work we tried to discover whether this quantity can significantly influence the behaviour of a spherical bubble, giving rise to observable phenomena in an experiment. Once a homobaric model deduced from RET theories was introduced, we analytically and numerically tested the equations in different conditions, always keeping in mind the comparison with what is known in the literature. The results are clear and surprising: in the presence of small-sized bubbles subject to a driving frequency of the order of 1 MHz, the presence of dynamic pressure can modify 1) the value of the generalized polytropic index, 2) the oscillation amplitude of the bubble and consequently temperature and heat flux, 3) the resonance effects both in amplitude and in frequency, 4) the maximum radius and the typical bounces of the sonoluminescence regime. These promising results are particularly interesting in the case of CO_2 for which large bulk viscosities are known in the literature and which exhibits sonoluminescence-inhibiting behaviour. In the future it will be important to continue these studies by making the model more realistic, starting from the case of specific heats dependent on temperature (non-polytropic gases[54]) and from the mass exchange effects in the gas-liquid interface. Unfortunately, to our knowledge, only very few experimental data are currently available on the oscillations of a CO_2 bubble, but we hope that there will soon be the possibility of a comparison between theory and experiments in different regimes, both for a verification of what has been obtained in this work and for an indirect measurement of the bulk viscosity value. Moreover, for engineering and medical applications, it is fundamental to move to a multi-bubble scenario, considering on the one hand bubbly liquids and on the other hand cavitation phenomena in soft tissues typical of the biological and bioengineering framework: we are already working on this point. In the future, knowledge of the effects associated with high values of bulk viscosity will be crucial for gaining better control over physical phenomena and for choosing the gas to be used inside the bubbles optimally.

ACKNOWLEDGMENTS

The authors would like to thank the anonymous reviewers for their helpful comments and suggestions. The paper was supported by Gruppo Nazionale di Fisica Matematica (GNFM) dell'INdAM and in part (F.B.) by the Italian research Project PRIN 2022 CUP: D53D23003020006 "The Mathematics and Mechanics of Nonlinear Wave Propagation in Solids".

REFERENCES

[1] L. Rayleigh, "On the pressure developed in a liquid during the collapse of a spherical cavity," Phyl. Mag. **34**, 94 (1917).
[2] R. Loefstedt, B. P. Barber, and S. J. Putterman, "Toward a hydrodynamic theory of sonoluminescence," Phys. Fluids A **5**, 2911 (1993).
[3] T. G. Leighton, *The acoustic bubble* (Academic Press, 1994).
[4] B. P. Barber, R. A. Hiller, S. J. Putterman, and K. R. Weninger, "Defining the unknowns of sonoluminescence," Phys. Reports **281**, 65 (1997).
[5] S. Hilgenfeldt, S. Grossmann, and D. Lohse, "Sonoluminescence light emission," Phys. Fluids **11**, 1318 (1999).
[6] A. Prosperetti and Y. Hao, "Modelling of spherical gas bubble oscillations and sonoluminescence," Phil. Trans. Royal Soc. A **357**, 203 (1999).
[7] S. J. Putterman and K. R. Weninger, "Sonoluminescence: How bubbles turns sound into light," Annu. Rev. Fluid Mech. **32**, 445

(2000).
[8] M. P. Brenner, S. Hilgenfeldt, and D. Lohse, "Single-bubble sonoluminescence," Rev. Mod. Phys.. **74**, 425 (2002).
[9] W. Lauterborn and T. Kurz, "Physics of bubble oscillations," Rep. Prog. Phys. **73**, 106501 (2010).
[10] G. Zhou and A. Prosperetti, "Modelling the thermal behaviour of gas bubbles," J. Fluid Mechanics **901**, R3 (2020).
[11] C. E. Brennen, "Cavitation in medicine," Interface Focus **5**, 20150022 (2015).
[12] K. Christensen-Jeffries, O. Couture, P. A. Dayton, Y. C. Eldar, K. Hynynen, F. Kiessling, M. O'Reilly, G. F. Pinton, G. Schmitz, M. X. Tang, M. Tanter, and R. J. van Sloun, "Super-resolution ultrasound imaging," Ultrasound Med. Biol. **46**, 865 (2020).
[13] S. P. Fletcher, A. Chisholm, M. Lavelle, R. Guthier, Y. Zhang, C. Power, R. Berbeco, and N. McDonald, "A study combining microbubble-mediated focused ultrasound and radiation therapy in the healthy rat brain and a F98 glioma model," Scientific Rep. **14**, 4831 (2024).
[14] N. Lapin, K. Gill, B. R. Shah, and R. Chopra, "Consistent opening of the blood brain barrier using focused ultrasound with constant intravenous infusion of microbubble agent," Scientific Rep. **10**, 16546 (2020).
[15] P. R. Gogate and A. M. Kabady, "A revew of applications of cavitation in biochemical engineering/biotechnology," Biochem. Eng. J. **44**, 60 (2009).
[16] D. Lohse, "Bubble puzzle: from fundamentals to applications," Phys. Rev. Fluids **3**, 110504 (2018).
[17] P. Koukovinis and M. Gavaises, eds., *Cavitation and bubble dynamics: fundamental and applications* (London Academic Press, 2021).
[18] X. Huang, G. Niu, Y. Xie, X. Chen, H. Hu, and G. Pan, "Application of ultrasonic cavitation in ship and marine engineering," J. Mar. Sci. Appl. **23**, 23 (2024).
[19] M. S. Plesset, "The dynamics of cavitation bubbles," J. Appl. Mech. **16**, 277 (1949).
[20] J. B. Keller and M. Miksis, "Bubble oscillations of large amplitude," J. Acoust. Soc. Am. **68**, 628 (1980).
[21] W. Lauterborn, "Numerical investigation of nonlinear oscillations of gas bubbles liquid," J. Acoust. Soc. Am. **59**, 283 (1976).
[22] F. Denner and S. Schenke, "Modeling acoustic emissions and shock formation of cavitation bubbles," Phys. Fluids **55**, 012114 (2023).
[23] A. Prosperetti, "Thermal effects and damping mechanisms in the forced radial oscillations of gas bubbles in liquid," J. Acoust. Soc. Am. **61**, 17 (1977).
[24] A. Prosperetti, "The thermal behaviour of oscillating gas bubbles," J. Fluid Mech. **222**, 587 (1991).
[25] C. C. Wu and P. H. Roberts, "A model of sonoluminescence," Proc. R.Soc. Lon. A **445**, 323 (1994).
[26] V. Q. Vuong, A. J. Szeri, and D. A. Young, "Shock formation within sonoluminescence bubbles," Phys. Fluids **11**, 10 (2001).
[27] T. Kamei, T. Kanagawa, and T. Ayukai, "An exhaustive theoretical analysis of thermal effect inside bubbles for weakly nonlinear pressure waves in bubbly liquids," Phys. Fluids **33**, 053302 (2021).
[28] S. Taniguchi, T. Arima, T. Ruggeri, and M. Sugiyama, "Effect of dynamic pressure on the shock structure in a rarefied polyatomic gas," Phys. Fluids **26**, 016103 (2014).
[29] S. Kosuge and K. Aoki, "Shock-wave structure for a polyatomic gas with large bulk viscosity," Phys. Rev. Fluids **3**, 023401 (2018).
[30] T. Ruggeri and S. Taniguchi, "Effect of dynamic pressure on the shock structure and sub-shock formation of a mixture of polyatomic gases," Comm. Appl. Math. Comput. (2023), https://doi.org/10.1007/s42967-023-00320-7.
[31] T. Arima, E. Barbera, F. Brini, and M. Sugiyama, "The role of the dynamic pressure in stationary heat conduction of a rarefied polyatomic gas," Phys. Lett. A **378**, 2695 (2014).
[32] E. Barbera, F. Brini, and M. Sugiyama, "Heat transfer problem in a van der Waals gas," Acta Appl. Math. **132**, 41 (2014).
[33] T. Arima, S. Taniguchi, T. Ruggeri, and M. Sugiyama, "Extended thermodynamics of real gases with dynamic pressure: An extension of Meixner's theory," Phys. Lett. A **44**, 2799 (2012).
[34] T. Arima and M. Sugiyama, "A novel effect of dynamic pressure on a nonequilibrium flow of a rarefied polyatomic gas through a diverging nozzle," Phys. Lett. A **476**, 128881 (2023).
[35] E. Touber, "Small-scale two dimensional turbulence shaped by bulk viscosity," J. Fluid Mech. **875**, 974 (2019).
[36] G. Emanuel, "Effect of bulk viscosity on a hypersonic boundary layer," Phys. Fluid A Fluid Dyn. **4**, 491 (1992).
[37] T. K. Sengupta, A. Sengupta, N. Sharma, A. Bhole, and K. Shurti, "Roles of bulk viscosity on Rayleigh-Taylor instability. Non-equilibrium thermodynamics due to spatio-temporal pressure fronts," Phys. Fluids **28**, 094102 (2016).
[38] Y. Peng, C. Peng, T. Nguyen, T. Sun, T. Porter, N. McDannold, J. N. Kheir, and B. Polizzotti, "Engineering caged microbubbles for controlled acoustic cavitation and pressure sensing," ACS Materials Letters **3**, 978 (2021).
[39] C. Boeije, P. Zitha, and A. Plyumakers, "High-speed imaging of degassing kinetics of CO2–water mixtures," Phy. Fluids **34**, 123307 (2022).
[40] Y. Shin, L. Deike, and L. Romero, "Modulation of bubble-mediated CO2 gas transfer due to wave-current interactions." Geoph. Research Letters **49**, e2022GL100017 (2022).
[41] S. M. Montazeri, N. Kalogerakis, and G. Kollipoulos, "CO2 nanobubbles as a novel kinetic promoter in hydrate-based desalination," Desalination **574**, 117296 (2024).
[42] A. Bouakaz and J. M. Escoffre, "From concept to early clinical trials: 30 years of microbubble-based ultrasound-mediated drug delivery research," Adv. Drug Delivery Rev. **206**, 115199 (2024).
[43] K. I. F. de Jong and P. W. de Leeuw, "Venous carbon dioxide embolism during laparoscopic cholecystectomy a literature review," European J. Int. Med. **60**, 9 (2019).
[44] F. Brini and L. Seccia, "Acceleration waves and oscillating gas bubbles modelled by rational extended thermodynamics," Proc. Royal Soc. A **478**, 2022.0246 (2022).
[45] I. Mueller and T. Ruggeri, *Rational Extended Thermodynamics* (New York - Springer, 1998).
[46] T. Ruggeri and M. Sugiyama, *Classical and Relativistic Rational Extended Thermodynamics of gases* (New York - Springer, 2021).
[47] Y. A. G. Man and F. J. Trujillo, "A new pressure formulation for gas-compressibility dampening in bubble dynamics models," Ultrasound Sonochem. **32**, 247 (2016).
[48] H. Lin, B. Storey, and A. J. Szeri, "Inertially driven inhomogeneities in violently collapsing bubbles: the validity of the Rayleigh-Plesset equation," J. Fluid Mech. **452**, 145 (2002).
[49] D. F. Gaitan, L. A. Crum, C. C. Church, and R. Roy, "Sonoluminescence and bubble dynamics for a single, stable, cavitation bubble," J. Acoust. Soc. Am. **91**, 3166 (1992).
[50] M. S. Plesset and A. Prosperetti, "Bubble dynamics and cavitation," Annu. Rev. Fluid Mech. **9**, 145 (1977).
[51] F. R. Gilmore, "The growth or collapse of a spherical bubble in a viscous compressible liquid," Report, Hydrodynamics laboratory, California Institue of Technology, California, USA **26-4**

(1952).
[52] A. M. Zhang, S. M. Li, P. Cui, and S. Li, "A unified theory for bubble dynamics," Phys. Fluids **35**, 033323 (2023).
[53] T. Arima, S. Taniguchi, T. Ruggeri, and M. Sugiyama, "Extended thermodynamics of dense gases," Cont. Mech. Thermodyn. **24**, 219 (2012).
[54] T. Arima, M. Carrisi, S. Pennisi, and T. Ruggeri, "Which moments are appropriate to describe gases with internal structure in rational extended thermodynamics?" Int. J. Non-lin. Mech. **137**, 103820 (2021).
[55] J. F. Bourgat, L. Desvillettes, P. L. Tallec, and B. Perthame, "Microreversible collisions for polyatomic gases." Eur. J. Mech. B/Fluids **13**, 237 (1994).
[56] F. Brini and T. Ruggeri, "Hyperbolicity of first and second order extended thermodynamics theory of polyatomic rarefied gases," Int. J. Non-lin. Mech. **124**, 103517 (2020).
[57] M. Bisi, T. Ruggeri, and G. Spiga, "Dynamical pressure in a polyatomic gas: interplay between kinetic theory and extended thermodynamics," Kinet. Relat. Models **11**, 71 (2018).
[58] I. Mueller and W. Mueller, *Fundamentals of thermodynamics and applications* (New York - Springer, 2009).
[59] F. Brini and L. Seccia, "Acceleration waves in cylindrical shrinking gas bubbles," Nucl. Science Engin. **197**, 2301 (2023).
[60] B. Sharma and R. Kumar, "Estimation of bulk viscosity of dilute gases using a nonequilibrium molecular dynamics approach," Phys. Rev. E. **100**, 013309 (2019).
[61] M. S. Cramer, "Numerical estimates for the bulk viscosity of ideal gases," Phys. Fluids **24**, 066102 (2012).
[62] F. J. O. K. Matar and E. A. Mueller, "Bulk viscosity of molecular fluids," J. of Chem. Phys. **148**, 174504 (2018).
[63] E. Kustova, M. Mekhonoshina, and A. Kosareva, "Relaxation processes in carbon dioxide," Phys. Fluids **31**, 046104 (2019).
[64] A. S. Meijer, A. S. de Wijn, M. F. E. Peters, N. J. Dam, and W. van de Water, "Coherent Rayleigh–Brillouin scattering measurements of bulk viscosity of polar and nonpolar gases, and kinetic theory," J. Chem. Phys. **133**, 164315 (2010).
[65] Y. Wang, W. Ubachs, and W. van de Water, "Bulk viscosity of CO2 from Rayleigh- Brillouin light scattering spectroscopy at 532 nm," J. Chem. Phys. **150**, 154502 (2019).
[66] J. R. Rumble, *CRC Handbook of Chemistry and Physics* (CRC Press, Boca Raton, FL, 2022).
[67] C. Shearwood and P. A. Sloan, "The Ruechardt experiment revisited: using simple theory, accurate measurement and python based data analysis," Eur. J. Phys.. **44**, 035102 (2023).
[68] S. Kumari, M. Keswani, S. Singh, M. Beck, E. Liebscher, P. Deymier, and S. Raghavan, "Control of sonoluminescence signal in deionized water using carbon dioxide," Microelectronic Engin. **88**, 3437 (2011).
[69] O. R. Enriquez, C. Sun, D. Lohse, A. Prosperetti, and D. van der Meer, "The quasi-static growth of CO2 bubbles," J. Fluid Mech. **741**, R1 (2014).
[70] M. Minnaert, "On musical air-bubbles and the sounds of running water," Phil. Mag. Ser. 7 **16**, 235 (1933).
[71] H. Frenzel and H. Schultes, "Luminescenz im ultraschallbeschickten Wasser," Zeit. Phys. Chemie **B27**, 421 (1934).